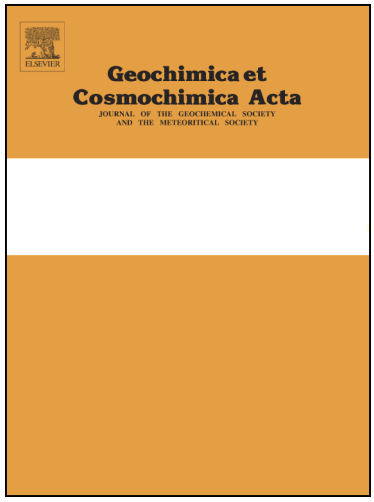

Rapid Cenozoic ingrowth of isotopic signatures simulating "HIMU" in ancient lithospheric mantle: Distinguishing source from process

Alex J. McCoy-West, Vickie C. Bennett, Yuri Amelin

PII: S0016-7037(16)30246-0
DOI: http://dx.doi.org/10.1016/j.gca.2016.05.013
Reference: GCA 9762

To appear in: *Geochimica et Cosmochimica Acta*

Received Date: 10 November 2015
Accepted Date: 5 May 2016

Please cite this article as: McCoy-West, A.J., Bennett, V.C., Amelin, Y., Rapid Cenozoic ingrowth of isotopic signatures simulating "HIMU" in ancient lithospheric mantle: Distinguishing source from process, *Geochimica et Cosmochimica Acta* (2016), doi: http://dx.doi.org/10.1016/j.gca.2016.05.013

Rapid Cenozoic ingrowth of isotopic signatures simulating "HIMU" in ancient lithospheric mantle: Distinguishing source from process

Alex J. McCoy-West[1*], Vickie C. Bennett[1] and Yuri Amelin[1]

[1]Research School of Earth Sciences, Australian National University, Canberra, 2601, Australia

[*] Present address: Department of Earth Sciences, Durham University, Durham, DH1 3LE, UK

Number of words: 7713

Number of references: 97

Number of figures: 10

Number of tables: 2

Corresponding author: Alex McCoy-West (alex.mccoywest@gmail.com)

ABSTRACT

Chemical and isotopic heterogeneities in the lithospheric mantle are increasingly being recognised on all scales of examination, although the mechanisms responsible for generating this variability are still poorly understood. To investigate the relative behavior of different isotopic systems in off-cratonic mantle, and specifically the origin of the regional southwest Pacific "HIMU" (high time integrated $^{238}U/^{204}Pb$) Pb isotopic signature, we present the first U-Th-Pb, Rb-Sr, Sm-Nd and Re-Os isotopic dataset for spinel peridotite xenoliths sampling the subcontinental lithospheric mantle (SCLM) beneath Zealandia. Strongly metasomatised xenoliths converge to a restricted range of Sr and Nd isotopic compositions ($^{87}Sr/^{86}Sr$ =0.7028-0.7033; ε_{Nd} ≈+3-+6) reflecting pervasive overprinting of their original melt depletion signatures by carbonatite-rich melts. In contrast, rare, weakly metasomatised samples possess radiogenic Nd isotopic compositions (ε_{Nd} >+15) and unradiogenic Sr isotopic compositions ($^{87}Sr/^{86}Sr$ <0.7022). This is consistent with melt extraction at ca. 2.0 Ga and in accord with widespread Paleoproterozoic Re-Os model ages from both weakly metasomatised and the more numerous, strongly metasomatised xenoliths. The coupling of chalcophile (Os), and lithophile (Sr and Nd) melt depletion ages from peridotite xenoliths on a regional scale under Zealandia argues for preservation of a significant mantle keel (•2 million km^3) associated with a large-scale Paleoproterozoic melting event. Lead isotopic compositions are highly variable with $^{206}Pb/^{204}Pb$ = 17.3-21.3 (n = 34) and two further samples with more extreme compositions of 22.4 and 25.4, but are not correlated with other isotopic data or U/Pb and Th/Pb ratios in either strongly or weakly metasomatised xenoliths; this signature is thus a recent addition to the lithospheric mantle. Lead model ages suggest that this metasomatism occurred in the last 200 m.y., with errorchrons from individual localities providing ages younger than 116 Ma. When considered in the regional tectonic context the Pb isotopic signatures are best explained through interaction of the lithospheric mantle with a weak

upwelling mantle plume that contained carbonatitic domains at ca. 110-115 Ma. Projection of the measured high U/Pb and Th/Pb signatures into the future predicts extreme Pb isotopic values distinct from any recognised terrestrial reservoir. We suggest that this type of young, carbonatite-related radiogenic Pb signature with extreme $^{238}U/^{204}Pb$ and $^{232}Th/^{204}Pb$, which is widely observed in the southwest Pacific, may reflect a secular change in mantle chemistry consistent with the increased prevalence of carbonatite sources during the Phanerozoic. This signature is referred to as "CarboHIMU", to differentiate it from the originally defined HIMU representing an ancient lower mantle component present in some ocean island basalts.

Keywords: Sr-Nd-Pb isotopes; HIMU; carbonatite; New Zealand; mantle xenoliths.

1. INTRODUCTION

Debate continues on the origin of isotopic signatures preserved in the lithospheric mantle as sampled by xenoliths, particularly as to the relationship between siderophile and chalcophile (Pb, Os) isotopic signatures, which may be carried largely in trace phases such as sulfides and metal alloys and lithophile (Sr, Nd) isotopic signatures that are hosted in major phases, which may be overprinted by crustally derived fluids. Understanding the mechanisms responsible for generating the observed isotopic heterogeneities and decoupling of isotopic systems, has widespread implications for mantle evolution as well as significance for how we interpret ages of lithospheric mantle events as determined from different isotopic systems. Related to this are key questions of if, and to what degree, a genetic link exists between signatures in the lower mantle and sub-continental lithospheric mantle (SCLM) and under what conditions these signatures are transferred.

In the southwest Pacific, Zealandia, the broader New Zealand micro-continent, is a largely submerged continental ribbon (>3.5×10^6 km^2) formed during terrane accretion at the eastern margin of Gondwana during the Phanerozoic from ca. 520-100 Ma. Present-day New Zealand comprises a complex collage of geological terranes (Fig. 1), of which the Cambrian to Early Cretaceous basement is divided into two major provinces (Mortimer, 2004): the older early Paleozoic Western Province composed of Gondwanan continental foreland, and the younger (late Paleozoic to mid-Cretaceous) Eastern Province that comprises predominantly deformed meta-greywackes that were accreted during a series of collisional events. These two provinces are separated by the Median Batholith, a long-lived arc-root plutonic complex that records the history of subduction related volcanism from the Carboniferous to Late Cretaceous at the Pacific margin of Gondwana (Mortimer et al., 1999). Intraplate basalts erupted sporadically throughout Zealandia over the last 100 m.y. are notable for their large range ($^{206}Pb/^{204}Pb$ = 18.2-20.9) and some highly radiogenic Pb isotopic ratios ($^{206}Pb/^{204}Pb$

>20.5; McCoy-West et al., 2010; Panter et al., 2006; Timm et al., 2010) and generally unradiogenic $^{87}Sr/^{86}Sr$ <0.704. Their SCLM source has been variously referred to as containing HIMU, HIMU-like or enriched mantle components.

Here we present new coupled U-Th-Pb, Rb-Sr, and Sm-Nd isotopic measurements combined with published Re-Os isotopic evidence obtained from the same samples (McCoy-West et al., 2013) for a regional suite of mantle xenoliths from throughout Zealandia including the Chatham Islands (Fig. 1). The goals of this study are, firstly, to investigate the relative behaviours of the chalcophile and lithophile element isotopic systems in recording lithosphere formation and modification events in this off-cratonic region, and, secondly, to use integrated geologic and isotopic observations to determine the origin and age of the widespread radiogenic Pb "HIMU" isotopic signature observed in the SCLM and derivative basalts throughout the southwest Pacific.

As originally defined, the HIMU (high time integrated $^{238}U/^{204}Pb$ or high-μ; Zindler and Hart, 1986) mantle end-member represents the component with the most radiogenic Pb isotopic signatures ($^{206}Pb/^{204}Pb$ >20.5) observed in OIB (ocean island basalts) and with relatively unradiogenic $^{87}Sr/^{86}Sr$ (<0.703). OIB with HIMU signatures are rare; the classic localities of St Helena in the Atlantic Ocean and some of the Cook-Austral islands (e.g. Mangaia, Tubaii and Rurutu) in the Pacific Ocean, although being characterised by high $^{206}Pb/^{204}Pb$, also have low $^{208}Pb/^{206}Pb$ ratios, similar to those of MORB (mid-ocean ridge basalts), requiring low time-integrated Th/U ratios and high time-integrated U/Pb and Th/Pb ratios, unlike those of any other mantle components (Stracke et al., 2005). Various mechanisms have been proposed for generating HIMU signatures in the mantle including early core formation, delamination of the SCLM and metasomatism by CO_2 rich fluids (e.g. McKenzie and O'Nions, 1983; Meijer et al., 1990; Nakamura and Tatsumoto, 1988; Vidal and Dosso, 1978), although more recently there has been a consensus that recycled ancient

oceanic lithosphere is involved in their formation (e.g. Chauvel et al., 1992; Hofmann, 2003; Hofmann and White, 1982; Stracke et al., 2003; Stracke et al., 2005; Weaver, 1991; Woodhead, 1996). Quantitative modelling has shown that modification of the oceanic lithosphere during subduction leads to substantial Pb loss compared to both U and Th and a preferential leaching of U relative to Th (Kelley et al., 2005; Stracke et al., 2003). Thus following subduction modification it is possible to generate a source with the appropriate U-Th-Pb ratios that following extended storage (ca. 0.5-3 Ga) in the lower mantle will develop HIMU characteristics (Chauvel et al., 1992; Hofmann and White, 1982; Stracke et al., 2003). While some authors still use HIMU in the originally defined sense (e.g. Stracke et al., 2005), it is increasingly common to use the term "HIMU" or HIMU-like to describe all basalts with $^{206}Pb/^{204}Pb > 19.5$ without full consideration of the genetic implications.

2. METHODS

Details of the acid leaching, chemical separation and mass spectrometry procedures are provided in the Electronic Annex and summarised here. Rubidium-Sr, Sm-Nd and U-Th-Pb concentrations and isotopic compositions were measured at the Australian National University. Whole rock powders were prepared using an agate ring mill, with clinopyroxene separates obtained from larger xenoliths using standard mineral separation techniques. Prior to digestion, all samples were sequentially leached in dilute HNO_3 and hot 6M HCl using a protocol comparable to that recommended by Wittig et al. (2009). Following acid leaching, mixed ^{85}Rb-^{84}Sr, ^{149}Sm-^{150}Nd spikes and a synthetic ^{233}U-^{236}U-^{229}Th-^{202}Pb-^{205}Pb double spike (Amelin et al., 2010) were added to the samples. This was followed by HF-HNO_3 digestion in sealed Teflon beakers on a hotplate at 130 °C. After the samples were completely dissolved, U-Th and Pb were separated using dilute HBr-anion exchange chromatography following the methods of Amelin (2008). Rubidium, Sr and the rare earth elements (REE) were then

sequentially separated from the remaining solution using cation exchange chromatography. Strontium was further purified using Sr-spec resin, and Sm and Nd were separated from the REE fraction using Ln-Spec resin.

Strontium, Nd, Sm and Pb isotopic compositions were determined by static collection on Faraday cups using a Triton Plus thermal ionisation mass spectrometer (TIMS). Rubidium isotopic compositions were measured in static collection mode on a MAT 261 TIMS. Reproducibility of reference standards throughout the analytical campaign (2σ population) was as follows: 10-100 ng aliquots of SRM987 $^{87}Sr/^{86}Sr = 0.710242 \pm 17$ (n = 12); 50-100 ng aliquots of an in-house Nd standard GSC AMES $^{143}Nd/^{144}Nd = 0.511977 \pm 10$ (n = 15) and $^{149}Sm/^{152}Sm = 0.516853 \pm 19$ (n = 11); 1 ng of SRM981 $^{206}Pb/^{204}Pb = 16.940 \pm 18$, $^{207}Pb/^{204}Pb = 15.497 \pm 13$ and $^{208}Pb/^{204}Pb = 36.711 \pm 55$ (n = 13). Uranium and Th concentrations were measured using an Aridus II desolvating nebuliser coupled to a Neptune Plus multi-collector ICP-MS. Analytical blanks in this study were in all cases negligible with no corrections applied. Replicate digestions of rock standard BCR-2 are within error of published Sr-Nd-Pb isotopic values; isotopic compositions of peridotite standards DTS-1 and PCC-1 are in good agreement with the limited published values (Table EA1).

3. SAMPLES AND RESULTS

Mantle xenoliths were collected from 13 localities from throughout Zealandia, including the North, South and Chatham Islands (Fig. 1). Petrographic descriptions, mineral chemistry, whole rock major and trace element concentrations including the platinum group elements and Re-Os isotopic data for all of these samples are available in McCoy-West et al. (2013; 2015). The xenoliths are predominantly harzburgites or clinopyroxene-poor lherzolites and are exclusively from the spinel-facies with equilibration temperatures varying between 830 and 1020 °C (McCoy-West et al., 2015). They represent a variably depleted portion of off-

cratonic SCLM with Al_2O_3 varying from 0.1-3.4 wt % that has undergone 3-28% melting ($F_{Yb\ in\ WR}$; McCoy-West et al., 2015). Unradiogenic Os isotopic compositions (McCoy-West et al., 2013) for a geographically restricted subset of xenoliths (the Waitaha domain; Fig. 1) that have Re depletion model ages and Re-Os age relationships in accord with widespread melt depletion at ca. 1.9 Ga have established the existence of a large region (>2 million km^3) of Paleoproterozoic SCLM beneath New Zealand (McCoy-West et al., 2015; McCoy-West et al., 2013). In contrast, samples from other regions of Zealandia are characterised by having heterogeneous Os isotopic compositions and Re-depletion ages and lacking correlations on Re/Os versus $^{187}Os/^{188}Os$ diagrams (Liu et al., 2015; McCoy-West et al., 2013). Strongly metasomatised xenoliths dominate the xenolith collection, with trace element signatures of clinopyroxene having been interpreted to reflect widespread interaction with a carbonatite component in the SCLM under Zealandia (McCoy-West et al., 2015; Scott et al., 2014a; 2014b).

3.1. The effect of acid leaching on Sr-Nd-Pb isotopes

Numerous studies of mantle xenoliths have demonstrated that owing to the ubiquitous presence of exogenic Pb combined with the low concentrations (i.e. sub 10 ppb) in unmetasomatised mantle materials, leaching is required to achieve meaningful U-Th-Pb ratios and Pb isotopic compositions (Wittig et al., 2009). A wide range of leaching protocols have previously been implemented (Hamelin and Allègre, 1988; McDonough and Chauvel, 1991; Pearson et al., 1993; Wittig et al., 2009). While leaching procedures using an HF step can result in severe fractionation of U-Th-Pb ratios, more moderate leaching using only HCl and HNO_3 as employed here, has not been shown to cause disturbance of parent-daughter ratios (see review in Wittig et al., 2009). After leaching, residues measured by TIMS typically contain comparable concentrations to the average of 8-14 unleached crystals measured by laser ablation (McCoy-West et al., 2015; Fig. 2). As seen in previous studies, leaching of

clinopyroxene removes a significant fraction (up to 99% of the Pb), with most of this being exogenous anthropogenic Pb. In this study, the proportion of the U, Th and Pb removed during leaching varies significantly (ca. 5-99 %; although it is a strong function of the concentration of the element in the sample; Table EA3; Fig. EA2). Parent-daughter ratios for the majority of samples plot on a 1:1 line (U/Pb; Sm/Nd; Fig. 2), showing that leaching prior to TIMS analysis has not fractionated their parent-daughter ratios. The Pb isotopic compositions of the measured leachates and residues also form a mixing line with Broken Hill Pb (Cooper et al., 1969), the pervasive anthropogenic Pb component seen throughout Australasia, consistent with the progressive removal of exogenous Pb during leaching (Fig. EA3). Further consideration of the effects of acid leaching on parent-daughter ratios and isotopic compositions are documented in the Electronic Annex.

3.2. Sr-Nd isotope data

The host basalts containing these xenoliths range in age from 86-1.8 Ma, with initial isotopic compositions for each xenolith calculated using the relevant eruption age. Initial $^{87}Sr/^{86}Sr$ compositions from all 34 xenoliths vary from 0.7019-0.7042 (excluding sample P43153b: $^{87}Sr/^{86}Sr = 0.7093$; Table 1) with 26 samples having a restricted $^{87}Sr/^{86}Sr$ range (0.7026-0.7032); no correlation is observed with $^{87}Rb/^{86}Sr$ (Fig. 3a). Replicate analyses of clinopyroxene from three fertile, weakly metasomatised samples preserve the most unradiogenic Sr signature (OU45852; DPP-1 & 5; $^{87}Sr/^{86}Sr = 0.7019$-0.7021). Initial $^{143}Nd/^{144}Nd$ compositions are more variable (0.5128-0.5142), with 9 samples having $^{143}Nd/^{144}Nd > 0.5130$ ($\varepsilon_{Nd} = +10$ - $+31$). There is no simple correlation between $^{143}Nd/^{144}Nd$ and $^{147}Sm/^{144}Nd$ (Fig. 3b). In Sr-Nd isotope space the majority of Zealandian xenoliths plot within, or near to, the field defined by intraplate magmas from New Zealand (Fig. 4a), and overlap the area that represents the HIMU mantle end-member, as has been previously observed (Scott et al., 2014a; 2014b). The least metasomatised samples of this study, as for

example indicated by La/Yb_N <1 (Fig. 5), however, preserve significant variability in both Sr and Nd isotopic compositions expanding the previously observed ranges based on predominantly metasomatised samples.

3.3. U-Th-Pb isotope data

Measured Pb isotopic compositions are highly variable (e.g. $^{206}Pb/^{204}Pb$ = 17.25-25.42; Table 2), although the majority of the xenoliths from the Waitaha domain and Chatham Islands exhibit a more restricted range of $^{206}Pb/^{204}Pb$ = 19.5-20.7 (Fig. 4). Lead isotopic ratios are uncorrelated with the abundance of their parent radionuclides (i.e. ^{238}U and ^{232}Th; Fig. 6a-b), and show no simple correlations with radiogenic effects in either other lithophile (Nd; Fig. 6c) or chalcophile (Os; Fig. 6d) isotope systems. The $^{238}U/^{204}Pb$ values of the Zealandia xenoliths range from 0.69 to 552, with 16 of 22 samples from the Waitaha domain having $^{238}U/^{204}Pb$ >45, a value that is significantly higher than in basalts from Mangaia, the most radiogenic example of classical HIMU OIB localities ($^{238}U/^{204}Pb$ = 26-39; Woodhead, 1996). In plots of $^{207}Pb/^{204}Pb$ and $^{208}Pb/^{204}Pb$ versus $^{206}Pb/^{204}Pb$ the data form a linear array that extends from compositions similar to the classic HIMU mantle component to less radiogenic compositions (Fig. 4c-d), with the majority of xenoliths having compositions comparable to New Zealand alkaline intraplate magmas (Fig. 4), which include the carbonatites of the Alpine Dyke Swarm ($^{206}Pb/^{204}Pb$ = 19.9-20.3; Barreiro and Cooper, 1987). These basalts show variability based on their location, with Chatham Island basalts consistently having the highest $^{206}Pb/^{204}Pb$ (19.7-20.8; Panter et al., 2006; Sprung et al., 2007; Timm et al., 2010). Whereas, the xenoliths from the same location record more variable compositions ($^{206}Pb/^{204}Pb$ = 19.5-22.4; Table 2), and elevated $^{207}Pb/^{204}Pb$ at a given $^{206}Pb/^{204}Pb$ relative to xenoliths from the Waitaha domain (Fig. 4c). To the west of the Alpine Fault, xenoliths consistently have the lowest Pb isotopic compositions within Zealandia; in accord with the Pb isotopic compositions of intraplate basalts especially those from the North Island (e.g. Cook et al., 2005; McGee et al., 2013),

211 which show a greater similarity to MORB compositions with low $^{206}Pb/^{204}Pb$ and $^{87}Sr/^{86}Sr$,
212 and relatively high ε_{Nd} (i.e. >+6).

213 **4. DISCUSSION**

214 **4.1. Evidence for multiple Paleoproterozoic to Cenozoic melt depletion events recorded**
215 **by chalcophile and lithophile isotopes**

216 *4.1.1. Re-Os ages*

217 Osmium isotopic compositions are often considered the most robust means of placing age
218 constraints on melting events in the SCLM (e.g. Handler et al., 1997; 2003; Liu et al., 2011;
219 Reisberg and Lorand, 1995; Walker et al., 1989). However, there is continued debate over the
220 meaning of Os model ages in the context of recycling of ancient heterogeneities preserved in
221 the oceanic mantle, perhaps in the form of sulfides or alloys. Liu et al. (2015) report Os
222 isotopic compositions of 14 xenoliths from two Alpine Dyke Swarm localities in West Otago
223 (Fig. 1) that have T_{RD} ages ranging from 0.5-2.1 Ga, with two further xenoliths from Lake
224 Wanaka preserving Archean T_{RD} ages of 2.7 Ga. They suggest that the highly depleted
225 craton-like mantle (forsterite mean = 92.3; n = 19; Scott et al., 2014b) underlying West Otago
226 is a mixture of ancient depleted domains and ambient residual mantle that has undergone
227 recent melting prior to being accreted to the SCLM (Liu et al., 2015). This localised
228 occurrence of Archean mantle contrasts with the Os compositions of xenoliths from the
229 Waitaha domain underlying East Otago (McCoy-West et al., 2013), an extensive region
230 (>55,000 km^2) of more fertile SCLM (Fo mean = 90.5; n = 27). The Waitaha domain consists
231 of 7 geographically coherent localities where 16 of 18 samples possess Paleoproterozoic ages,
232 as indicated by a combination of Os model ages, Re-Os isochrons and a regional
233 aluminochron, consistent with widespread melt depletion at 1.9 Ga (McCoy-West et al., 2015;
234 2013). Waitaha domain xenoliths also possess coherent platinum group element patterns that

require both a relatively simple melting history and the long-term preservation of their original mantle sulfides (McCoy-West et al., 2015).

4.1.2. Sm-Nd model ages

The radiogenic $^{143}Nd/^{144}Nd$ ($\varepsilon Nd > +30$) of some samples from the Waitaha domain is in accord with ancient melt depletion. Neodymium model ages were only calculated for samples that are weakly metasomatised or unmetasomatised ($La/Yb_N < 1$), to avoid spurious ages produced by late stage metasomatism. T_{CHUR} and T_{DM} ages represent maximum and minimum ages, respectively (Table 1). These samples provide T_{CHUR} model ages varying between 0.1 and 3.5 Ga (n = 10), with three samples (and two duplicates) from within the Waitaha domain recording Nd model ages of 1.5-2.7 Ga (e.g. DPP-3, WFP-2 and WFP-8), consistent with the regional Paleoproterozoic melting age based on Re-Os systematics (McCoy-West et al., 2015; 2013). Additionally, the steepest array in Sm-Nd isotopic space provides a minimum estimate of the timing of this ancient melting event at >1525 Ma (Fig. 3; Fig. EA5a). Furthermore, lithophile evidence for this ancient melting event is observed in the dataset of Scott et al. (2014b) with two xenoliths having $\varepsilon Nd > +20$, and two different xenoliths having $\varepsilon Hf > 100$, again consistent with them being residues of Proterozoic melt depletion (>1.5 Ga).

Interrogating the record for younger melt depletion events is more complicated. Several unmetasomatised samples from the Trig L locality have high $^{147}Sm/^{144}Nd$ (>0.4; Fig. 3) and produce T_{CHUR} model ages from 130-380 Ma indicative of a secondary Paleozoic-Mesozoic melting event. The two samples that produce the youngest ages provide a 2-point age regression of 108 ± 8 Ma (Fig. EA5b). These samples are chemically distinct from the main cluster of metasomatised samples (Fig. 3) and combined with two additional similar xenoliths from Trig L in the dataset of Scott et al. (2014b) provide an 'isochron' age of 131 ± 33 Ma (Fig. EA5b). This is consistent with generation during an Early Cretaceous melting event (ca. 131-108 Ma). The remaining model ages between 0.5 and 1.5 Ga could be: 1) the

result of additional melting events, although it is impossible to distinguish these based on the lithophile isotope data alone; or 2) mixed ages resulting from the variable contributions of ancient melting and more recent events (i.e. large amounts of Paleoproterozoic melting and only weak Cretaceous melting will result in model ages >1 Ga).

4.1.3. Additional Sr-Pb evidence for Paleoproterozoic melt extraction

Strontium isotopic compositions are not widely used for determining ancient melt depletion events as Rb and Sr compositions of xenoliths are readily overprinted by interaction with high Rb/Sr crustal fluids containing radiogenic Sr. Although within the Zealandian xenoliths $^{87}Sr/^{86}Sr$ compositions are unsupported by their $^{87}Rb/^{86}Sr$, a significant number of samples still contain unradiogenic $^{87}Sr/^{86}Sr$ (<0.7030), with three replicated clinopyroxene separates preserving $^{87}Sr/^{86}Sr$ of 0.7019-0.7021, additionally two xenoliths analysed by Scott et al. (2014b) have $^{87}Sr/^{86}Sr$ <0.7022. These are among the least radiogenic Sr isotopic compositions preserved in xenoliths worldwide. In a similar manner as for Re depletion ages (e.g. Shirey and Walker, 1998) used in the Re-Os system and for the similar reason that both Re and Rb are readily overprinted by enriched crustal fluids, it is possible to calculate Rb depletion model ages. Using a depleted mantle source ($^{87}Rb/^{86}Sr = 0.0188$; $^{87}Sr/^{86}Sr = 0.7026$; Workman and Hart, 2005) and assuming that all of the Rb was lost during the melting event (i.e. analogous to a T_{RD} Re-Os age and similarly providing a minimum age of melt depletion). All 6, low $^{87}Sr/^{86}Sr$, samples yield similar Rb depletion model ages of ca. 2.0 Ga (1.91- 2.40 Ga), consistent with the Paleoproterozoic melting event recorded by Os and Nd isotopic data. Comparable evidence for Proterozoic melt extraction is found in peridotite xenoliths from Central Asia (Mongolia and Vitim) that preserve similarly unradiogenic Sr isotope compositions ($^{87}Sr/^{86}Sr = 0.7017$-0.7022) and coupled Sr-Nd and Os model ages of ca. 2 Ga (Ionov et al., 2005; Pearson et al., 2004; Stosch et al., 1986). Additionally two of the low $^{87}Sr/^{86}Sr$ Zealandia samples have the most unradiogenic Pb isotopic compositions measured

($^{207}Pb/^{204}Pb$ = 15.36-15.37); these compositions require ancient melting without subsequent interaction with a metasomatic agent. Thus only in the rare, unmetasomatised samples do the Re-Os, U-Pb, Rb-Sr and Sm-Nd systems all record the same Paleoproterozoic melting event. If this SCLM was the result of recent upwelling and accretion of heterogeneous asthenospheric mantle to the lithosphere, these lithophile isotope signatures would likely have been obliterated. Rather, these rare samples provide strong evidence that the widespread Paleoproterozoic Os model ages from the Waitaha domain xenoliths record a regional melting event affecting all isotopic systems. For the majority of the xenoliths however, the lithophile isotope systems have been more heavily overprinted during later metasomatism.

4.2. Determining the signature of the metasomatic agent

Notable positive Th-U and Sr anomalies and large fractionations of Nb/Ta and Ti/Eu in clinopyroxene have been used to demonstrate that a widespread region of the SCLM of southern Zealandia has been variably modified by interaction with a carbonatitic component (McCoy-West et al., 2015; Scott et al., 2014a; 2014b). A strong correlation is observed between the strength of this metasomatism, as for example reflected in LREE patterns and the level of isotopic heterogeneity (Fig. 5). The least metasomatised xenoliths (La/Yb_N <1) are exclusively from the Waitaha domain and preserve highly heterogeneous Sr-Nd-Pb isotopic compositions ($^{87}Sr/^{86}Sr$ = 0.7019-0.7044; ε_{Nd} = 4-32; $^{206}Pb/^{204}Pb$ =17.2-21.3). Whereas, strongly metasomatised samples (i.e. Chatham Islands samples with secondary clinopyroxene and La/Yb_N = 2.9-23.2) possess significantly less isotopic variability and converge to compositions similar to carbonatites found in the Alpine Dyke Swarm (Barreiro and Cooper, 1987) and pristine oceanic carbonatites (Hoernle et al., 2002; Mourão et al., 2012). Therefore, the Sr and Nd isotopic composition of the metasomatic agent can be estimated due to the restricted range of $^{87}Sr/^{86}Sr$ and ε_{Nd} within the metasomatised xenoliths with a composition of

309 $^{87}Sr/^{86}Sr = 0.70305 \pm 25$; $\varepsilon_{Nd} = +4.5 \pm 1.5$ (Fig. 5) and in agreement with independent
310 estimates of Scott et al. (2014b).

311 In contrast, Pb isotopic compositions of even the most metasomatised samples
312 maintain a significant range (Fig. 5c; $^{206}Pb/^{204}Pb$ =19.5-21). The lack of complete
313 overprinting, as has been the case for Sr and Nd, can be related to the dual lithophile and
314 chalcophile characteristics of Pb. Sulfides have previously been advocated as the source of the
315 missing Pb in the silicate mantle (Hart and Gaetani, 2006; Meijer et al., 1990), with included
316 sulfides in abyssal peridotites preserving direct evidence of long-lived Os and Pb isotopic
317 heterogeneities in the mantle (Burton et al., 2012). Although no direct estimates of the rate of
318 Pb diffusion in sulfides are available, Pb is highly compatible in sulfide with estimates of D_{Pb}
319 sulfide/silicate of ca. 2000 (Burton et al., 2012; Gaetani and Grove, 1999). Additionally, the
320 low temperatures of the Zealandian SCLM ca. 800-1050 °C (McCoy-West et al., 2015; Scott
321 et al., 2014b) and of the metasomatic agent (carbonatite magmas erupt at <550 °C; Krafft and
322 Keller, 1989) will further limit any diffusion. Thus, the Pb isotopic compositions of the
323 metasomatised xenoliths are considered a mixture of the compositions of the original included
324 sulfides and the overprinting carbonatite. This provides a mechanism of *in situ* decoupling of
325 lithophile and chalcophile isotopic signatures with Sr-Nd compositions dominated by the
326 metasomatic signature and Os dominated by the sulphide and/or metal alloys, whereas Pb
327 records a mixed signature when mantle sulfides are preserved.

328 **4.3. Age constraints on the widespread metasomatic signature**

329 Previous estimates on the emplacement of this metasomatic signature in the SCLM are highly
330 variable, but most suggest that the metasomatism occurred during the Phanerozoic between
331 ca. 500-100 Ma (e.g. Handler et al., 2003; Hart et al., 1997; Panter et al., 2006; 2000; Rocchi
332 et al., 2002; Scott et al., 2014a; Zhang and O'Reilly, 1997), and prior to the mid-Cretaceous
333 separation of New Zealand from Antarctica. However, placing strict time constraints on the

334 emplacement of this radiogenic Pb signature in the SCLM is complicated because: 1) it is
335 unlikely that the xenoliths were in isotopic equilibrium immediately prior to the metasomatic
336 event; and 2) the preservation of variable amounts of mantle sulfides aids in the development
337 of Pb isotopic heterogeneities unrelated to the metasomatic agent.

338 *4.3.1. Pb model ages of metasomatism*

339 If we assume the least metasomatised samples in the suite with the lowest $^{238}U/^{204}Pb$ and
340 $^{232}Th/^{204}Pb$ values preserve pre-metasomatism isotopic ratios (e.g. OU45852 and WTL-1;
341 Table 2), and that the current distinctive U-Th/Pb signature was imparted during
342 metasomatism, we can calculate the length of time required to evolve the isotopic signature
343 observed in the metasomatised xenoliths (i.e. T_{Meta} ages). Calculated T_{Meta} ages for the
344 samples, assuming the initial isotopic composition of the region is similar to that of OU45852
345 ($^{206}Pb/^{204}Pb = 19.568$; $^{208}Pb/^{204}Pb = 39.056$), using both the ^{238}U-^{206}Pb and ^{232}Th-^{208}Pb
346 systems are generally in good agreement (Table 2; Fig. 7a). These ages are only indicative,
347 but show radiogenic Pb signatures can evolve very rapidly in the SCLM and that this
348 metasomatism is a recent event (<180 Ma), with the majority of T_{Meta} age estimates from the
349 Waitaha domain ≤120 Ma (n = 15/19; Fig. 7a).

350 *4.3.2. Rapid ingrowth of Pb isotopic signatures*

351 A more robust way of assessing when this metasomatic signature was emplaced into the
352 SCLM is to look at individual xenolith localities separately, because prior to metasomatism
353 they probably contained samples closer to isotopic equilibrium. For example, the Chatham
354 Islands are located ca. 1500 km away from mainland New Zealand and do not record the
355 Paleoproterozoic melting event observed in the Waitaha domain. Errorchron ages using the
356 U-Th-Pb chronometers (^{238}U-^{206}Pb, ^{235}U-^{207}Pb and ^{232}Th-^{208}Pb) have been calculated using
357 whole rock and clinopyroxene data from four localities throughout Zealandia and agree within
358 error at individual localities (Table 3; Fig. 8). As we can exclude mixing, i.e. there is no

359 known reservoir with the required radiogenic ($^{206}Pb/^{204}Pb$ >25) endmember Pb composition,
360 the errorchrons are considered to provide age information, but should be interpreted with
361 caution. All-inclusive ages include all samples from a locality and often have large errors
362 (>50 Ma) and exceedingly high MSWDs >>100 (Table 3), suggesting they do not represent a
363 single population and a secondary factor has perturbed the isotopic composition of some
364 samples. Therefore, preferred ages have also been calculated from those samples considered
365 to have been in isotopic equilibrium prior to the metasomatism (Fig. 8). The ages discussed
366 below are preferred ages, however, both preferred and all-inclusive ages agree within error
367 and the interpretation outlined is independent of which ages are selected.
368 Whole rock samples from the Chatham Islands produce 4-point U-Th-Pb errorchrons
369 that yield similar ages and are consistent with metasomatism having occurred from ca. 110-
370 120 Ma (e.g. ^{238}U-^{206}Pb = 110 ± 9 Ma; Table 3; Fig. 8). Further evidence that this
371 metasomatism occurred at ca. 100-120 Ma in the Chatham Islands is provided by the Rb-Sr
372 and Sm-Nd regressions, which provide similar ages (Fig. EA5; Rb-Sr = 117 ± 40 Ma; Sm-Nd
373 = 100 ± 38 Ma), although with large errors due the small range of parent-daughter ratios
374 ($^{87}Rb/^{86}Sr$ = 0.007-0.17; $^{147}Sm/^{144}Nd$ = 0.12-0.18). Within the Waitaha domain due to the
375 large range of parent-daughter ratios (e.g. $^{238}U/^{204}Pb$ = 0.7-552; Fig. 6; Table 2), highly
376 radiogenic Pb isotope ratios can be ingrown vary rapidly. The most radiogenic sample within
377 the xenolith suite WFP-1 ($^{206}Pb/^{204}Pb$ = 25.42; $^{208}Pb/^{204}Pb$ = 47.28) also possesses
378 exceptionally elevated $^{238}U/^{204}Pb$ and $^{232}Th/^{204}Pb$ at 473 and 2320, respectively. Construction
379 of U-Th-Pb errorchrons for samples from the Fortification Peak locality shows that this
380 composition would require only ca. 67-74 Ma to develop (e.g. ^{232}Th-^{208}Pb = 67 ± 6; Fig. 8).
381 Xenoliths from the Pilot Point and Trig L localities are consistent with even younger
382 metasomatism with ingrowth of the observed compositions requiring only ca. 28-42 Ma and
383 ca. 24-36 Ma, respectively.

The errorchron ages presented here demonstrate that regions of the SCLM with extremely high U/Pb and Th/Pb as observed in the Zealandian mantle can rapidly evolve to extremely radiogenic Pb isotopic compositions. We suggest ages from the Chatham Islands are consistent with this distinctive U-Th-Pb signature being added to the SCLM after ca. 120-110 Ma (Figs. 7 & 8; Fig. EA5), but immediately prior to the cessation of subduction along the eastern Gondwana margin (e.g. the youngest dated I-type granite in New Zealand is 105 ± 1 Ma; Tulloch and Kimbrough, 2003). Isotopic systematics from three localities within the Waitaha domain require even younger ages from ca. 70-30 Ma for the ingrowth of the metasomatic signature. This metasomatism has likely been ongoing with the continuous re-activation of the fossilised metasomatic signature (Fig. 7b) through interaction with the sporadic basaltic melts that have traversed the SCLM over the last 100 Ma (McCoy-West et al., 2010; Timm et al., 2010). In summary, the errorchron ages range from ca. 120 to 30 Ma and are consistent with this metasomatism being young and likely to have occurred within the last ca. 120 Ma. Within the current precision, however, it is not possible to resolve definitely whether the metasomatic signature was added primarily in a distinct event prior to the cessation of subduction or whether it reflects an average of processes over the last ca. 100 Ma.

4.4. Origins of the radiogenic Pb signature simulating "HIMU" in the lithospheric mantle

The existence of a widespread HIMU-like signature ($^{206}Pb/^{204}Pb > 19.5$) in the southwest Pacific as observed in intraplate basalts has been extensively investigated (Finn et al., 2005; Hoernle et al., 2006; McCoy-West et al., 2010; Panter et al., 2006; 2000; Timm et al., 2009; 2010), although whether this component resides in the asthenosphere or SCLM has remained controversial. The Pb isotopic compositions of mantle xenoliths from throughout Zealandia preserve similar signatures ($^{206}Pb/^{204}Pb$ ca. 19.5-21.5; Fig. 4) allowing us to directly assess the origin of this "HIMU" signature in the SCLM and whether it is genetically related to a long-

lived component in the mantle, i.e. HIMU, or is the result of more recent interaction with additional fluids or melts. Taking into account the tectonic history of Zealandia, several processes may have been responsible for the generating this regional "HIMU"-like component. These are: 1) isolation of an ancient (> 2 Ga) HIMU domain in the SCLM without secondary modification; 2) overprinting of the xenoliths by the intraplate magmatism during entrainment and eruption of the xenoliths; 3) metasomatism associated with long-lived subduction at the eastern margin of Gondwana during the Phanerozoic; and 4) the interaction of a upwelling mantle with the SCLM immediately prior to and during Gondwana break-up as proposed in some tectonic models (Hart et al., 1997; Storey et al., 1999; Weaver et al., 1994).

4.4.1. An ancient HIMU component

The generation of the distinctive composition of the HIMU mantle end-member requires a specific combination of time integrated elevated U/Pb and Th/Pb and also elevated U/Th for extended periods of time (ca. >0.5 Ga). Although the present day isotopic compositions of Zealandian xenoliths are consistent with a HIMU-like component (Fig. 4) their Pb isotopic ratios are unsupported by their parent-daughter ratios (Fig. 6a-b). When comparing the U-Th/Pb systematics of samples from the Waitaha domain (Table 2; $^{238}U/^{204}Pb$ = 0.7-552; $^{232}Th/^{204}Pb$ = 0.5-2658) to the archetypal end-member of classical HIMU (i.e. Mangaia: $^{238}U/^{204}Pb$ = 32.6 ± 3.5; $^{232}Th/^{204}Pb$ = 124 ± 11; Woodhead, 1996) the former has significantly greater ranges, with the variability in the HIMU end-member, assuming an origin from 0.5-3.0 Ga recycled oceanic crust only increasing to $^{238}U/^{204}Pb$ = 12-61 and $^{232}Th/^{204}Pb$ = 45-177 (Stracke et al., 2003). A significant number of Waitaha domain samples (n = 17) extend to considerably higher $^{238}U/^{204}Pb$ and $^{232}Th/^{204}Pb$ values than required to generate even the youngest (500 Ma) HIMU signatures (Fig. 6). If this signature resulted from *in situ* ingrowth a much stronger correlation with isotopic composition would be expected due to the large range of parent-daughter ratios. Furthermore, there is no correlation between the Pb isotopic

compositions and either the Nd or Os isotopic compositions (Fig. 6), which preserve evidence of Paleoproterozoic melt depletion. Therefore this signature is unrelated to a long-lived mantle component in the SCLM.

4.4.2. Basalt infiltration

During partial melting of the mantle, lithophile elements are strongly concentrated, by up to several orders of magnitude, in the melt phase relative to residual peridotite. Thus contamination of xenoliths during transportation and entrainment within a basaltic melt may be a possible source of the radiogenic Pb signature. However, several lines of evidence argue against this: 1) leaching of clinopyroxene separates from the xenoliths has shown that the most radiogenic Pb is preserved within the crystals and is not the result of grain boundary contamination (Fig. EA1); 2) the isotopic compositions of the xenoliths and their host intraplate basalts (Panter et al., 2006; Timm et al., 2009; 2010) are similar (Table EA4) and therefore irrespective of the higher Pb concentrations in the melts, isotopic mixing will have little impact; 3) mass balance modelling of trace element budgets has shown that the majority of xenoliths, can only accommodate very small amounts of basalt infiltration (≤0.1 %; McCoy-West et al., 2015) and 4) comparison of Pb metasomatic model ages derived from the xenoliths with host basalt eruption ages suggests that the metasomatism generally occurred over an extended period prior to xenolith entrainment (Fig. 7b), rather than at the time of eruption.

4.4.3. Distinguishing between subduction and plume contributions

Here we propose a model for the origin of the isotopic characteristics of the Zealandian SCLM incorporating elements of the tectonic history of Zealandia (Fig. 11), although the exact cause of rifting between Zealandia and Marie Byrd Land remains unclear, having previously been attributed to a range of processes varying from subducted slab capture (Luyendyk, 1995) to the impingement of a weak mantle plume on the SCLM (Hart et al.,

459 1997). A long-lived subduction zone was present at the eastern margin of Gondwana,
460 outboard of the proto-New Zealand from ca. 520-105 Ma (McCoy-West et al., 2014; Muir et
461 al., 1994, 1996; 1998; Tulloch and Kimbrough, 2003). Invoking this subduction system as the
462 source of the distinctive Pb isotopic systematics of the SCLM in the southwest Pacific is
463 straightforward, as has been argued previously for alkaline intraplate magmas (Panter et al.,
464 2006), however, no current models adequately explain why the locus of rifting did not occur
465 within the West Antarctic Rift System, the largest continental rift system observed on Earth
466 that contains extensively thinned continental crust (Rocchi et al., 2002; Winberry and
467 Anandakrishnan, 2004). Although there are advocates for plume driven rifting, arguments
468 against a Late Cretaceous plume are based on the lack of large-scale regional uplift
469 (LeMasurier and Landis, 1996), the much lower than expected magma production rates
470 relative to common plume-related flood basalt provinces (Finn et al., 2005), and the
471 complexity of resolving the effects of impingement of an upwelling mantle plume head on the
472 subducted oceanic lithosphere.

473 Isotopic evidence in mantle xenoliths for subduction being responsible for imparting
474 this signature into the SCLM is less compelling. During subduction, oceanic crust undergoes
475 significant dewatering, which lowers the solidus and generates melting in the mantle wedge,
476 such that any SCLM located above this region for a significant period of time will be
477 chemically modified by interaction with fluids or melts. Sr isotopic compositions of the
478 SCLM are easily perturbed by interaction with crustal fluids or melts and in the off-cratonic
479 mantle are volumetrically dominated by elevated $^{87}Sr/^{86}Sr$ >0.704 (e.g. Ionov et al., 2002;
480 2006; Liu et al., 2012; Witt-Eickschen et al., 2003). Whereas a significant number of
481 Zealandian xenoliths exhibit unradiogenic $^{87}Sr/^{86}Sr$ (<0.703; n = 18; Table 1), which requires
482 isolation from fluids derived from altered subducted oceanic crust or the likely overlying
483 Gondwanan derived sedimentary detritus (i.e. sediments comparable to the Late Mesozoic

quartzo-feldspathic greywackes that dominate the Eastern Province: $^{87}Sr/^{86}Sr$ = 0.708-0.720; Adams et al., 2002). It is not possible to entirely eliminate that the SCLM has been isolated from subduction zones fluids, rather the fluids may have been generated in an intra-oceanic subduction zone resulting in extremely unradiogenic compositions. Subduction at the eastern margin of Gondwana was long-lived (ca. 520-105 Ma) and uniformitarianism would suggest that if this process was ongoing for >100 m.y. a much more widespread and regionally homogeneous distribution of this radiogenic Pb signature would be expected along the paleo-subduction margin, however, in eastern Australia this signature is not observed (i.e. $^{206}Pb/^{204}Pb$ <19.5; Nasir et al., 2010; Paul et al., 2005; Zhang et al., 2001). Instead, tectonic reconstructions prior to Gondwana break-up show a somewhat concentric distribution of this HIMU-like Pb composition centred around the boundary between the Campbell Plateau and Marie Byrd Land (i.e. an elongate bullseye: see Fig. 8 in Finn et al., 2005), consistent with the impingement of upwelling mantle on the SCLM, that was constrained within the mantle wedge and therefore spread parallel to the trench axis. Additionally, due to the large range in $^{238}U/^{204}Pb$ and $^{232}Th/^{204}Pb$ values within the Zealandian mantle xenoliths, which can evolve to very distinctive compositions in <100 m.y. (see *5.3*), significantly more Pb isotopic heterogeneity would be expected if subduction was responsible for imparting this metasomatic signature over an extended period of the Phanerozoic (>400 m.y.). Furthermore, the distinctive clinopyroxene trace element patterns (McCoy-West et al., 2015; Scott et al., 2014b) observed within Zealandian mantle xenoliths are incompatible with generation by subduction zone fluids (i.e. lack of fractionation between U and Th) and have instead been attributed to carbonatite metasomatism (McCoy-West et al., 2015; Scott et al., 2014a; 2014b). Isotopic evidence is also consistent with a carbonatite component as: 1) the main cluster of strongly metasomatised xenoliths have similar isotopic compositions as measured in unmodified oceanic carbonatites (Fig. 5); and 2) the unradiogenic $^{87}Sr/^{86}Sr$

observed in Waitaha xenoliths requires that the metasomatic agent is low in Rb, another common feature of carbonatites (Hoernle et al., 2002; Ray et al., 2000). Carbonatite metasomatism is highly effective at transporting large ion lithophile elements such as U (Green and Wallace, 1988), and in some weakly metasomatised samples small volume fractionations have produced extreme $^{238}U/^{204}Pb$ ratios with the samples rapidly developing negative Δ7/4 (Fig. 9; Δ207Pb/204Pb; Hart, 1984) as they evolve along a trajectory away from the mantle array (see Fig. 10). Samples with the most negative Δ7/4 also possess strongly fractionated Nb/Ta in their clinopyroxene (Fig. 9), as would be expected from disequilibrium interactions with a carbonatitic agent (Green et al., 1992). Carbonatites erupted within the Alpine Dyke Swarm could possibly represent the carbonatitic metasomatic agent, however, it is not possible to rigorously assess this due to the lack of coupled U-Th and Pb isotopic data (Barreiro and Cooper, 1987; Cooper, 1986; Cooper and Paterson, 2008) for this suite.

Although controversial, the involvement of upwelling mantle, possibly in the form of a plume feature, has been suggested to have been involved in the separation of Zealandia from West Antarctica (Hart et al., 1997; Kipf et al., 2014; Lanyon et al., 1993; Storey et al., 1999; Sutherland et al., 2010; Weaver et al., 1994). Weaver *et al.* (1994) placed the axis of their proposed plume at the reconstructed boundary between the Campbell Plateau and Marie Byrd Land, intersecting the region defined by the most radiogenic Pb values ($^{206}Pb/^{204}Pb$ >20.5) prior to Gondwana break-up (Finn et al., 2005; Panter et al., 2006) and adjacent to the oldest oceanic crust observed between New Zealand and Antarctica (Laird and Bradshaw, 2004). The distinctive Pb isotopic signature of the Zealandian xenoliths is consistent with addition of this metasomatic signature to the SCLM in the Late Cretaceous sometime after ca. 120Ma (Fig. 8). Additionally, elevated $^{147}Sm/^{144}Nd$ and Nd isotopic compositions of three samples within the Waitaha domain, which are distinct from the composition of the metasomatic

agent, suggest a secondary melting event in the Early Cretaceous (ca. 131-108 Ma; Fig. EA5b). Disturbance of ancient Nd model ages in least metasomatised samples from the Waitaha domain is compatible with this melting event being widespread. During the Early Cretaceous the Pacific Plate reversed polarity and started moving slowly northwards (i.e. Aptian: 125-112 Ma; Bradshaw, 1989; Larson et al., 1992), with collision between the Hikurangi Plateau and the northern margin of Zealandia resulting in a cessation of subduction at ca. 105 Ma along this portion of the Gondwana margin (Davy et al., 2008; Hoernle et al., 2010; Mukasa and Dalziel, 2000). Extensional volcanism and major fault-bounded sedimentary basins developed shortly thereafter (i.e. Stitts Tuff: 101 ± 2 Ma; Muir et al., 1997), during a period of major crustal extension prior to the opening of the Tasman Sea. We suggest a combination of these processes weakened the subducting lithosphere and subsequently resulted in detachment of the slab allowing a pathway for upwelling mantle to interact with the SCLM (Fig. 11b). The impingement of this upwelling mantle on the lithosphere would have resulted in elevated heat flow, as recorded by the voluminous Separation Point Suite (>20,000 km^2) that was emplaced into the crust between ca. 120-110 Ma (Mortimer et al., 1997; Muir et al., 1994; 1997).

Therefore, on the basis of tectonic and isotopic evidence we propose that the most likely scenario is the radiogenic HIMU-like Pb signature was emplaced by carbonatite-rich low degree melts in the periphery of a large weak plume head that metasomatised the SCLM sometime after 120 Ma. This upwelling mantle either punched through a weakened subducted slab or was the catalyst for its detachment, although subduction had entirely ceased by ca. 105 Ma. During upwelling these carbonatite-rich melts variably metasomatised a widespread region of SCLM (ca. 5 million km^2; Fig. 11b). This metasomatism is possibly ongoing to the present day with the "fossilised" carbonatite signature remobilised when asthenospheric melts traverse the SCLM producing the distinctive intraplate magmas of Zealandia (Fig. 11d).

559 **4.5. Rapid ingrowth of signatures simulating "HIMU" and more heterogeneity in the**
560 **future**

561 The extreme range of $^{238}U/^{204}Pb$ and $^{232}Th/^{204}Pb$ observed in Zealandian xenoliths
562 unsupported by their Pb isotopic compositions (Fig. 6), requires the recent addition of this U-
563 Th enriched component to the SCLM. If undisturbed ingrowth of radiogenic Pb continues, a
564 previously unrecognised signature with extreme Pb isotopic compositions ("ultra HIMU")
565 will rapidly develop. Forward modelling of xenolith Pb isotopic compositions, using their
566 present day parent-daughter ratios is presented (Fig. 10; Table EA5). In the future the Waitaha
567 domain will possess a significantly more heterogeneous composition (i.e. in 200 m.y.
568 $^{206}Pb/^{204}Pb$ = 17.5-40.3), especially in $^{208}Pb/^{204}Pb$ versus $^{206}Pb/^{204}Pb$ isotopic space, due to the
569 variable Th/U of the samples. For comparison, *sensu stricto* HIMU samples from Mangaia
570 evolve as a coherent group and preserve higher $^{207}Pb/^{204}Pb$ (Fig. 10a), but after only ca. 150
571 m.y. some samples from the heterogeneous Waitaha domain will have both higher $^{206}Pb/^{204}Pb$
572 and $^{208}Pb/^{204}Pb$ (Fig. 10b). Outside of Zealandia, radiogenic Pb signatures in the off-cratonic
573 mantle are generally rare, see the xenolith compilation of Wittig et al. (2009; n = 350).
574 HIMU-like compositions attributed to carbonatite metasomatism are also observed in
575 peridotite xenoliths from the Atlas Mountains, Morocco (Marks et al., 2009; Wittig et al.,
576 2010). The Atlas xenoliths have a restricted range of Pb isotope compositions ($^{206}Pb/^{204}Pb$ =
577 19.98-20.25) and comparable $^{238}U/^{204}Pb$ and $^{232}Th/^{204}Pb$ to the main cluster of Zealandian
578 xenoliths (Fig. 6). Forward modelling done by Wittig et al. (2010) results in less radiogenic
579 compositions but a similar trajectory in $^{207}Pb/^{204}Pb$ versus $^{206}Pb/^{204}Pb$ space, although the Atlas
580 samples evolve more rapidly in $^{208}Pb/^{204}Pb$ space due to their higher Th/U (Fig. 10).
581 Additionally, a few studies have attributed the development of HIMU-like signatures in
582 continental intraplate basalts to radiogenic ingrowth within a carbonate metasomatised SCLM
583 (Janney et al., 2002; Tappe et al., 2007). The fact that this signature is not more widespread is

surprising, but could be attributed to: 1) the fortuitous rapid removal of this signature from the SCLM during subsequent melting events effectively removing the excess U and Th; or 2) the process of generating large fractionations in Th/Pb and U/Pb by carbonatite related metasomatism has only become widespread on the Phanerozoic Earth (64% of dated carbonatites are Phanerozoic in age, although this could be a preservation bias; Veizer et al., 1992; Wolley and Bailey, 2012), due to secular changes in the oxygen fugacity of the mantle (Evans, 2012; Shirey and Richardson, 2011; Tappe et al., 2014) that have increased carbonatite stability during interactions at the base of the SCLM.

Although the exact mechanism that imparted the radiogenic Pb signature into the SCLM in Zealandia may be debated, it has been demonstrated that this signature is young and has no genetic link with the classical HIMU mantle end-member observed in some OIB defined by Zindler & Hart (1986). Due to the antiquity of much of the sampled SCLM, its isotopic composition results from multiple melting and metasomatic events. Therefore, classifying samples from the SCLM using nomenclature originally intended for oceanic basalts has misleading connotations regarding the longevity of these signatures (i.e. heterogeneity within OIB and MORB is the result of the segregation of distinct components and 1-3 G.y. of storage in the deep mantle). Studies worldwide describe the presence of SCLM with HIMU affinities, largely based on the compositions of intraplate basalts (e.g. Panter et al., 2006; Rooney et al., 2014), although, whether any of these samples really contain an archetypal HIMU or are instead the result of recent interaction with a metasomatic agent remains unresolved. We suggest that the process recorded here whereby carbonatite metasomatism imparts extremely elevated parent-daughter ratios ($^{238}U/^{204}Pb$ >70; $^{232}Th/^{204}Pb$ >200) to regions of the SCLM be henceforth distinguished as CarboHIMU (i.e. carbonatite related high μ).

5. CONCLUSIONS

An integrated U-Th-Pb, Rb-Sr, Sm-Nd and Re-Os isotopic dataset for spinel peridotite xenoliths sampling the variably metasomatised SCLM beneath Zealandia, allows new insights into the formation of off-cratonic lithosphere and time constraints to be placed on the development of the "HIMU"-like signature observed throughout the southwest Pacific. Rare weakly metasomatised xenoliths preserve the coupling of chalcophile (Os) and lithophile (Sr and Nd) isotope compositions, all indicative of melt extraction at ca. 2.0 Ga. Furthermore, Paleoproterozoic Re-Os model ages are regionally widespread in the more abundant, strongly metasomatised xenoliths, with the lithophile isotopic signatures having been subsequently overprinted by carbonatite-rich melts. These observations are consistent with the formation and stabilisation of a voluminous region of SCLM ($\geq$2 million km^3) in a Paleoproterozoic melt depletion event and the preservation of this ancient mantle keel beneath a large portion of Zealandia today. This contrasts with interpretations from a localised occurrence of xenoliths with ancient (up to 2.7 Ga) Os model ages, decoupled from other isotopic systems, as mantle residues recycled from within the convecting mantle and later accreted to the SCLM (Liu et al., 2015). Lead isotope compositions are decoupled from the other isotopic data, with extreme $^{238}U/^{204}Pb$ and $^{232}Th/^{204}Pb$ values requiring this metasomatic signature to have been added to the SCLM in the Early Cretaceous and continuously reactivated by subsequent volcanism. We propose this distinctive radiogenic Pb signature was imparted into the SCLM by carbonate-rich low degree melts that heterogeneously metasomatised a widespread region of SCLM sometime after ca. 120 Ma, but prior to the onset of this type of volcanism at 98 Ma. If allowed to develop undisturbed into the future, the extreme U/Pb and Th/Pb characteristics of these samples will produce extreme Pb isotopic values distinct from any reservoir currently observed on Earth. We suggest the limited sampling of this signature in the rock record may reflect a secular change in mantle chemistry associated with the increased prevalence of

carbonatite sources within the mantle and that this unique metasomatic signature be referred to as CarboHIMU.

Acknowledgements

AMW was supported by an Australian Postgraduate Award and J.C. Jaeger Fellowship at the ANU. We thank S. Zink for lab support and T. Ireland and V. Salters for comments on an earlier draft. This manuscript was improved by constructive reviews by S. Tappe and two anonymous reviewers. We thank Dmitri Ionov for his editorial handling and constructive comments.

644 **REFERENCES**

645 Adams, C.J., Barley, M.E., Maas, R. and Doyle, M.G. (2002) Provenance of Permian-Triassic volcaniclastic
646 sedimentary terranes in New Zealand: Evidence from their radiogenic isotope characteristics and detrital mineral
647 age patterns. New Zealand Journal of Geology and Geophysics 45, 221-242.

648 Amelin, Y. (2008) The U–Pb systematics of angrite Sahara 99555. Geochimica et Cosmochimica Acta 72, 4874-
649 4885.

650 Amelin, Y., Kaltenbach, A., Iizuka, T., Stirling, C.H., Ireland, T.R., Petaev, M. and Jacobsen, S.B. (2010) U–Pb
651 chronology of the Solar System's oldest solids with variable $^{238}U/^{235}U$. Earth and Planetary Science Letters 300,
652 343-350.

653 Barreiro, B.A. and Cooper, A.F. (1987) A Sr, Nd, and Pb isotope study of alkaline lamprophyres and related
654 rocks from Westland and Otago, South Island, New Zealand. Geological Society of America Special Papers 215,
655 115-126.

656 Bradshaw, J.D. (1989) Cretaceous geotectonic patterns in the New-Zealand region. Tectonics 8, 803-820.

657 Burton, K.W., Cenki-Tok, B., Mokadem, F., Harvey, J., Gannoun, A., Alard, O. and Parkinson, I.J. (2012)
658 Unradiogenic lead in Earth/'s upper mantle. Nature Geosci 5, 570-573.

659 Chauvel, C., Hofmann, A.W. and Vidal, P. (1992) HIMU-EM: The French Polynesian connection. Earth and
660 Planetary Science Letters 110, 99-119.

661 Cook, C., Briggs, R.M., Smith, I.E.M. and Maas, R. (2005) Petrology and geochemistry of intraplate basalts in
662 the south Auckland volcanic field, New Zealand: Evidence for two coeval magma suites from distinct sources.
663 Journal of Petrology 46, 473-503.

664 Cooper, J.A., Reynolds, P.H. and Richards, J.R. (1969) Double-spike calibration of the Broken Hill standard
665 lead. Earth and Planetary Science Letters 6, 467-478.

666 Davy, B., Hoernle, K. and Werner, R. (2008) Hikurangi Plateau: Crustal structure, rifted formation, and
667 Gondwana subduction history. Geochemistry, Geophysics, Geosystems 9, Q07004.

668 Eagles, G., Gohl, K. and Larter, R.D. (2004) High-resolution animated tectonic reconstruction of the South
669 Pacific and West Antarctic margin. Geochemistry Geophysics Geosystems 5, Q07002,
670 doi:07010.01029/02003GC000657.

671 Evans, K.A. (2012) The redox budget of subduction zones. Earth-Science Reviews 113, 11-32.

672 Finn, C.A., Muller, R.D. and Panter, K.S. (2005) A Cenozoic diffuse alkaline magmatic province (DAMP) in the
673 southwest Pacific without rift or plume origin. Geochemistry Geophysics Geosystems 6, Q02005,
674 doi:02010.01029/02004GC000723.

675 Gaetani, G.A. and Grove, T.L. (1999) Wetting of mantle olivine by sulfide melt: implications for Re/Os ratios in
676 mantle peridotite and late-stage core formation. Earth and Planetary Science Letters 169, 147-163.

677 Green, D.H. and Wallace, L.M. (1988) Mantle metasomatism by ephemeral carbonatite melts. Nature 336, 459-
678 462.

679 Green, T.H., Adam, J. and Siel, S.H. (1992) Trace element partitioning between silicate minerals and carbonatite
680 at 25 kbar and application to mantle metasomatism. Mineralogy and Petrology 46, 179-184.

681 Hamelin, B. and Allègre, C.J. (1988) Lead isotope study of orogenic lherzolite massifs. Earth and Planetary
682 Science Letters 91, 117-131.

683 Handler, M.R., Bennett, V.C. and Esat, T.M. (1997) The persistence of off-cratonic lithospheric mantle: Os
684 isotopic systematics of variably metasomatised southeast Australian xenoliths. Earth and Planetary Science
685 Letters 151, 61-75.

686 Handler, M.R., Wysoczanski, R.J. and Gamble, J.A. (2003) Proterozoic lithosphere in Marie Byrd Land, West
687 Antarctica: Re-Os systematics of spinel peridotite xenoliths. Chemical Geology 196, 131-145.

688 Hart, S.R. (1984) A large-scale isotope anomaly in the Southern Hemisphere mantle. Nature 309, 753-757.

689 Hart, S.R., Blusztajn, J., LeMasurier, W.E. and Rex, D.C. (1997) Hobbs Coast Cenozoic volcanism: Implications
690 for the West Antarctic rift system. Chemical Geology 139, 223-248.

691 Hart, S.R. and Gaetani, G.A. (2006) Mantle Pb paradoxes: the sulfide solution. Contributions to Mineralogy and
692 Petrology 152, 295-308.

693 Hoernle, K., Hauff, F., van den Bogaard, P., Werner, R., Mortimer, N., Geldmacher, J., Garbe-Schönberg, D. and
694 Davy, B. (2010) Age and geochemistry of volcanic rocks from the Hikurangi and Manihiki oceanic Plateaus.
695 Geochimica et Cosmochimica Acta 74, 7196-7219.

696 Hoernle, K., Tilton, G., Le Bas, M., Duggen, S. and Garbe-Schönberg, D. (2002) Geochemistry of oceanic
697 carbonatites compared with continental carbonatites: Mantle recycling of oceanic crustal carbonate.
698 Contributions to Mineralogy and Petrology 142, 520-542.

699 Hoernle, K., White, J.D.L., van den Bogaard, P., Hauff, F., Coombs, D.S., Werner, R., Timm, C., Garbe-
700 Schönberg, D., Reay, A. and Cooper, A.F. (2006) Cenozoic intraplate volcanism on New Zealand: Upwelling
701 induced by lithospheric removal. Earth and Planetary Science Letters 248, 350-367.

702 Hofmann, A.W. (2003) Sampling mantle heterogeneity through oceanic basalts: Isotopes and trace elements,
703 Treatise of Geochemistry. Elsevier Ltd., pp. 61-101.

704 Hofmann, A.W. and White, W.M. (1982) Mantle plumes from ancient oceanic crust. Earth and Planetary Science
705 Letters 57, 421-436.

706 Huang, Y., Hawkesworth, C., Smith, I., van Calsteren, P. and Black, P. (2000) Geochemistry of late Cenozoic
707 basaltic volcanism in Northland and Coromandel, New Zealand: Implications for mantle enrichment processes.
708 Chemical Geology 164, 219-238.

709 Huang, Y., Hawkesworth, C., van Calsteren, P., Smith, I. and Black, P. (1997) Melt generation models for the
710 Auckland volcanic field, New Zealand: Constraints from U-Th isotopes. Earth and Planetary Science Letters
711 149, 67-84.

712 Ionov, D.A., Ashchepkov, I. and Jagoutz, E. (2005) The provenance of fertile off-craton lithospheric mantle: Sr–
713 Nd isotope and chemical composition of garnet and spinel peridotite xenoliths from Vitim, Siberia. Chemical
714 Geology 217, 41-75.

715 Ionov, D.A., Mukasa, S.B. and Bodinier, J.-L. (2002) Sr–Nd–Pb Isotopic Compositions of Peridotite Xenoliths
716 from Spitsbergen: Numerical Modelling Indicates Sr–Nd Decoupling in the Mantle by Melt Percolation
717 Metasomatism. Journal of Petrology 43, 2261-2278.

718 Ionov, D.A., Shirey, S.B., Weis, D. and Brügmann, G. (2006) Os-Hf-Sr-Nd isotope and PGE systematics of
719 spinel peridotite xenoliths from Tok, SE Siberian craton: Effects of pervasive metasomatism in shallow
720 refractory mantle. Earth and Planetary Science Letters 241, 47-64.

721 Jacobsen, S.B. and Wasserburg, G.J. (1984) Sm-Nd isotopic evolution of chondrites and achondrites, II. Earth
722 and Planetary Science Letters 67, 137-150.

723 Janney, P.E., Le Roex, A.P., Carlson, R.W. and Viljoen, K.S. (2002) A chemical and multi-isotope study of the
724 Western Cape Olivine Melilitite Province, South Africa: Implications for the sources of kimberlites and the
725 origin of the HIMU signature in Africa. Journal of Petrology 43, 2339-2370.

726 Kamp, P.J.J. (1986) The mid-Cenozoic Challenger Rift System of western New Zealand and its implications for
727 the age of Alpine fault inception. Geological Society of America Bulletin 97, 255-281.

728 Kelley, K.A., Plank, T., Farr, L., Ludden, J. and Staudigel, H. (2005) Subduction cycling of U, Th, and Pb. Earth
729 and Planetary Science Letters 234, 369-383.

730 Kimbrough, D.L., Mattinson, J.M., Coombs, D.S., Landis, C.A. and Johnston, M.R. (1992) Uranium-lead ages
731 from the Dun Mountain ophiolite belt and Brook Street terrane, South Island, New Zealand. Geological Society
732 of America Bulletin 104, 429-443.

733 Kipf, A., Hauff, F., Werner, R., Gohl, K., van den Bogaard, P., Hoernle, K., Maicher, D. and Klügel, A. (2014)
734 Seamounts off the West Antarctic margin: A case for non-hotspot driven intraplate volcanism. Gondwana
735 Research 25, 1660-1679.

736 Krafft, M. and Keller, J. (1989) Temperature measurements in carbonatite lava lakes and flows from Oldoinyo
737 Lengai, Tanzania. Science 245, 168-170.

738 Laird, M.G. and Bradshaw, J.D. (2004) The break-up of a long-term relationship: the Cretaceous separation of
739 New Zealand from Gondwana. Gondwana Research 7, 273-286.

740 Lanyon, R., Varne, R. and Crawford, A.J. (1993) Tasmanian Tertiary basalts, the Balleny plume, and opening of
741 the Tasman Sea (southwest Pacific Ocean). Geology 21, 555-558.

742 Larson, R.L., Steiner, M.B., Ebra, E. and Lancelot, Y. (1992) Paleolatitudes and tectonic reconstructions of the
743 oldest portion of the Pacific plate: A comparative study, Proceedings of the ocean drilling program: Scientific
744 results. College Station, Texas, pp. 615-631.

745 LeMasurier, W.E. and Landis, C.A. (1996) Mantle-plume activity recorded by low-relief erosion surfaces in
746 West Antarctica and New Zealand. Geological Society of America Bulletin 108, 1450-1466.

747 Liu, J., Carlson, R.W., Rudnick, R.L., Walker, R.J., Gao, S. and Wu, F.-y. (2012) Comparative Sr–Nd–Hf–Os–
748 Pb isotope systematics of xenolithic peridotites from Yangyuan, North China Craton: Additional evidence for a
749 Paleoproterozoic age. Chemical Geology 332–333, 1-14.

750 Liu, J., Rudnick, R.L., Walker, R.J., Gao, S., Wu, F.-y., Piccoli, P.M., Yuan, H., Xu, W.-l. and Xu, Y.-G. (2011)
751 Mapping lithospheric boundaries using Os isotopes of mantle xenoliths: An example from the North China
752 Craton. Geochimica et Cosmochimica Acta 75, 3881-3902.

753 Liu, J., Scott, J.M., Martin, C.E. and Pearson, D.G. (2015) The longevity of Archean mantle residues in the
754 convecting upper mantle and their role in young continent formation. Earth and Planetary Science Letters 424,
755 109-118.

756 Ludwig, K.R. (2008) Isoplot 3.71, 3.71 ed. Berkeley Geochronology Centre.

757 Luyendyk, B.P. (1995) Hypothesis for Cretaceous rifting of east Gondwana caused by subducted slab capture.
758 Geology 23, 373-376.

759 Marks, M.W., Neukirchen, F., Vennemann, T. and Markl, G. (2009) Textural, chemical, and isotopic effects of
760 late-magmatic carbonatitic fluids in the carbonatite–syenite Tamazeght complex, High Atlas Mountains,
761 Morocco. Mineralogy and Petrology 97, 23-42.

762 McCoy-West, A.J., Baker, J.A., Faure, K. and Wysoczanski, R. (2010) Petrogenesis and origins of mid-
763 Cretaceous continental intraplate volcanism in Marlborough, New Zealand: Implications for the long-lived
764 HIMU magmatic mega-province of the SW Pacific. Journal of Petrology 51, 2003-2045.

765 McCoy-West, A.J., Bennett, V.C., O'Neill, H.S.C., Hermann, J. and Puchtel, I.S. (2015) The interplay between
766 melting, refertilization and carbonatite metasomatism in off-cratonic lithospheric mantle under Zealandia: An
767 integrated major, trace and platinum group element study. Journal of Petrology 56, 563-604.

768 McCoy-West, A.J., Bennett, V.C., Puchtel, I.S. and Walker, R.J. (2013) Extreme persistence of cratonic
769 lithosphere in the Southwest Pacific: Paleoproterozoic Os isotopic signatures of Zealandia. Geology 41, 231-234.

770 McCoy-West, A.J., Mortimer, N. and Ireland, T.R. (2014) U–Pb geochronology of Permian plutonic rocks,
771 Longwood Range, New Zealand: implications for Median Batholith–Brook Street Terrane relations. New
772 Zealand Journal of Geology and Geophysics 57, 65-85.

773 McDonough, W.F. and Chauvel, C. (1991) Sample contamination explains the Pb isotopic composition of some
774 Rurutu island and Sasha seamount basalts. Earth and Planetary Science Letters 105, 397-404.

775 McGee, L.E., Smith, I.E.M., Millet, M.-A., Handley, H.K. and Lindsay, J.M. (2013) Asthenospheric control of
776 melting processes in a monogenetic basaltic system: A case study of the Auckland Volcanic Field, New Zealand.
777 Journal of Petrology 54, 2125-2153.

778 McKenzie, D. and O'Nions, R.K. (1983) Mantle reservoirs and ocean island basalts. Nature 301, 229-231.

779 Meijer, A., Kwon, T.T. and Tilton, G.R. (1990) U-Th-Pb partitioning behaviour during partial melting in the
780 upper mantle: implications for the origin of high Mu components and the 'Pb Paradox'. Journal of Geophysical
781 Research-Solid Earth and Planets 95, 433-448.

782 Meisel, T., Walker, R.J., Irving, A.J. and Lorand, J.-P. (2001) Osmium isotopic compositions of mantle
783 xenoliths: A global perspective. Geochimica et Cosmochimica Acta 65, 1311-1323.

784 Mortimer, N. (2004) New Zealand's geological foundations. Gondwana Research 7, 261-272.

785 Mortimer, N., Tulloch, A.J. and Ireland, T. (1997) Basement geology of Taranaki and Wanganui Basins, New
786 Zealand. New Zealand Journal of Geology and Geophysics 40, 223-236.

787 Mortimer, N., Tulloch, A.J., Spark, R.N., Walker, N.W., Ladley, E., Allibone, A. and Kimbrough, D.L. (1999)
788 Overview of the Median Batholith, New Zealand: A new interpretation of the geology of the Median Tectonic
789 Zone and adjacent rocks. Journal of African Earth Sciences 29, 257-268.

790 Mourão, C., Mata, J., Doucelance, R., Madeira, J., Millet, M.-A. and Moreira, M. (2012) Geochemical temporal
791 evolution of Brava Island magmatism: Constraints on the variability of Cape Verde mantle sources and on
792 carbonatite–silicate magma link. Chemical Geology 334, 44-61.

793 Muir, R.J., Ireland, T.R., Weaver, S.D. and Bradshaw, J.D. (1994) Ion microprobe U-Pb zircon geochronology of
794 granitic magmatism in the Western Province of the South Island, New Zealand. Chemical Geology 113, 171-189.

795 Muir, R.J., Ireland, T.R., Weaver, S.D. and Bradshaw, J.D. (1996) Ion microprobe dating of Paleozoic
796 granitoids: Devonian magmatism in New Zealand and correlations with Australia and Antarctica. Chemical
797 Geology 127, 191-210.

798 Muir, R.J., Ireland, T.R., Weaver, S.D., Bradshaw, J.D., Evans, J.A., Eby, G.N. and Shelley, D. (1998)
799 Geochronology and geochemistry of a Mesozoic magmatic arc system, Fiordland, New Zealand. Journal of the
800 Geological Society, London 155, 1037-1053.

801 Muir, R.J., Ireland, T.R., Weaver, S.D., Bradshaw, J.D., Waight, T.E., Jongens, R. and Eby, G.N. (1997)
802 SHRIMP U-Pb geochronology of Cretaceous magmatism in northwest Nelson-Westland, South Island, New
803 Zealand. New Zealand Journal of Geology and Geophysics 40, 453-463.

804 Mukasa, S.B. and Dalziel, I.W.D. (2000) Marie Byrd Land, West Antarctica: Evolution of Gondwana's Pacific
805 margin constrained by zircon U-Pb geochronology and feldspar common-Pb isotopic compositions. Geological
806 Society of America Bulletin 112, 611-627.

807 Nakamura, Y. and Tatsumoto, M. (1988) Pb, Nd, and Sr isotopic evidence for a multicomponent source for rocks
808 of Cook-Austral islands and hetrogeneities of mantle plumes. Geochimica et Cosmochimica Acta 52, 2909-2924.

Nasir, S.J., Everard, J.L., McClenaghan, M.P., Bombardieri, D. and Worthing, M.A. (2010) The petrology of high pressure xenoliths and associated Cenozoic basalts from Northeastern Tasmania. Lithos 118, 35-49.

Palme, H. and O'Neill, H.S.C. (2014) 3.1 - Cosmochemical estimates of mantle composition, in: Holland, H.D., Turekian, K.K. (Eds.), Treatise on Geochemistry (Second Edition). Elsevier, Oxford, pp. 1-39.

Panter, K.S., Blusztajn, J., Hart, S.R., Kyle, P.R., Esser, R. and McIntosh, W.C. (2006) The origin of HIMU in the SW Pacific: Evidence from intraplate volcanism in southern New Zealand and Subantarctic Islands. Journal of Petrology 47, 1673-1704.

Panter, K.S., Hart, S.R., Kyle, P., Blusztanjn, J. and Wilch, T. (2000) Geochemistry of Late Cenozoic basalts from the Crary Mountains: characterization of mantle sources in Marie Byrd Land, Antarctica. Chemical Geology 165, 215-241.

Paul, B., Hergt, J.M. and Woodhead, J.D. (2005) Mantle heterogeneity beneath the Cenozoic volcanic provinces of central Victoria inferred from trace-element and Sr, Nd, Pb and Hf isotope data. Aust. J. Earth Sci. 52, 243-260.

Pearson, D.G., Davies, G.R. and Nixon, P.H. (1993) Geochemical constraints on the petrogenesis of diamond facies pyroxenites from the Beni Bousera peridotite massif, North Morocco. Journal of Petrology 34, 125-172.

Pearson, D.G., Irvine, G.J., Ionov, D.A., Boyd, F.R. and Dreibus, G.E. (2004) Re-Os isotope systematics and platinum group element fractionation during mantle melt extraction: A study of massif and xenolith peridotite suites. Chemical Geology 208, 29-59.

Ray, J.S., Trivedi, J.R. and Dayal, A.M. (2000) Strontium isotope systematics of Amba Dongar and Sung Valley carbonatite-alkaline complexes, India: evidence for liquid immiscibility, crustal contamination and long-lived Rb/Sr enriched mantle sources. Journal of Asian Earth Sciences 18, 585-594.

Reisberg, L. and Lorand, J.P. (1995) Longevity of sub-continental mantle lithosphere from osmium isotope systematics in orogenic peridotite massifs. Nature 376, 159-162.

Rocchi, S., Armienti, P., D'Orazio, M., Tonarini, S., Wijbrans, J.R. and Di Vincenzo, G. (2002) Cenozoic magmatism in the western Ross Embayment: Role of mantle plume versus plate dynamics in the development of the West Antarctic Rift System. Journal of Geophysical Research: Solid Earth 107, 2195.

Rooney, T.O., Nelson, W.R., Dosso, L., Furman, T. and Hanan, B. (2014) The role of continental lithosphere metasomes in the production of HIMU-like magmatism on the northeast African and Arabian plates. Geology.

Scott, J.M., Hodgkinson, A., Palin, J.M., Waight, T.E., Meer, Q.H.A. and Cooper, A.F. (2014a) Ancient melt depletion overprinted by young carbonatitic metasomatism in the New Zealand lithospheric mantle. Contributions to Mineralogy and Petrology 167, 1-17.

Scott, J.M., Waight, T.E., van der Meer, Q.H.A., Palin, J.M., Cooper, A.F. and Münker, C. (2014b) Metasomatized ancient lithospheric mantle beneath the young Zealandia microcontinent and its role in HIMU-like intraplate magmatism. Geochemistry, Geophysics, Geosystems 15, 3477-3501.

Shirey, S.B. and Richardson, S.H. (2011) Start of the Wilson Cycle at 3 Ga Shown by Diamonds from Subcontinental Mantle. Science 333, 434-436.

Shirey, S.B. and Walker, R.J. (1998) The Re-Os isotope system in cosmochemistry and high-temperature geochemistry. Annual Reviews of Earth and Planetary Sciences 26, 423-500.

Sprung, P., Schuth, S., Munker, C. and Hoke, L. (2007) Intraplate volcanism in New Zealand: the role of fossil plume material and variable lithospheric properties. Contributions to Mineralogy and Petrology 153, 669-687.

Storey, B.C., Leat, P.T., Weaver, S.D., Pankhurst, R.J., Bradshaw, J.D. and Kelley, S. (1999) Mantle plumes and Antarctica-New Zealand rifting: evidence from the mid-Cretaceous mafic dykes. Journal of the Geological Society of London 156, 659-671.

852 Stosch, H.G., Lugmair, G.W. and Kovalenko, V.I. (1986) Spinel peridotite xenoliths from the Tariat Depression,
853 Mongolia. II: Geochemistry and Nd and Sr isotopic composition and their implications for the evolution of the
854 subcontinental lithosphere. Geochimica et Cosmochimica Acta 50, 2601-2614.

855 Stracke, A., Bizimis, M. and Salters, V.J.M. (2003) Recycling oceanic crust: Quantitative constraints.
856 Geochemistry, Geophysics, Geosystems 4, 8003.

857 Stracke, A., Hofmann, A.W. and Hart, S.R. (2005) FOZO, HIMU, and the rest of the mantle zoo. Geochemistry
858 Geophysics Geosystems 6.

859 Sutherland, R., Spasojevic, S. and Gurnis, M. (2010) Mantle upwelling after Gondwana subduction death
860 explains anomalous topography and subsidence histories of eastern New Zealand and West Antarctica. Geology
861 38, 155-158.

862 Tappe, S., Foley, S.F., Stracke, A., Romer, R.L., Kjarsgaard, B.A., Heaman, L.M. and Joyce, N. (2007) Craton
863 reactivation on the Labrador Sea margins: $^{40}Ar/^{39}Ar$ age and Sr–Nd–Hf–Pb isotope constraints from alkaline and
864 carbonatite intrusives. Earth and Planetary Science Letters 256, 433-454.

865 Tappe, S., Kjarsgaard, B.A., Kurszlaukis, S., Nowell, G.M. and Phillips, D. (2014) Petrology and Nd–Hf isotope
866 geochemistry of the Neoproterozoic Amon Kimberlite Sills, Baffin Island (Canada): Evidence for deep mantle
867 magmatic activity linked to supercontinent cycles. Journal of Petrology 55, 2003-2042.

868 Timm, C., Hoernle, K., Van Den Bogaard, P., Bindeman, I. and Weaver, S. (2009) Geochemical evolution of
869 intraplate volcanism at Banks Peninsula, New Zealand: Interaction between asthenospheric and lithospheric
870 melts. Journal of Petrology 50, 989-1023.

871 Timm, C., Hoernle, K., Werner, R., Hauff, F., den Bogaard, P.v., White, J., Mortimer, N. and Garbe-Schönberg,
872 D. (2010) Temporal and geochemical evolution of the Cenozoic intraplate volcanism of Zealandia. Earth Science
873 Reviews 98, 38-64.

874 Tulloch, A.J. and Kimbrough, D.L. (2003) Paired plutonic belts in convergent margins and the development of
875 high Sr/Y magmatism: Peninsular Ranges batholith of Baja-California and Median batholith of New Zealand, in:
876 Johnson, S.E., Paterson, S.R., Fletcher, J.M., Girty, G.H., Kimbrough, D.L., Martín-Barajas, A. (Eds.), Tectonic
877 evolution of northwestern México and the southwestern USA. Geological Society of America Special Paper 374,
878 Boulder, Colorado, pp. 275-295.

879 Veizer, J., Bell, K. and Jansen, S.L. (1992) Temporal distribution of carbonatites. Geology 20, 1147-1149.

880 Vidal, P. and Dosso, L. (1978) Core formation: catastrophic or continuous? Sr and Pb isotope geochemistry
881 constraints. Geophysical Research Letters 5, 169-172.

882 Walker, R.J., Carlson, R.W., Shirey, S.B. and Boyd, F.R. (1989) Os, Sr, Nd, and Pb isotope systematics of
883 southern African peridotite xenoliths: Implications for the chemical evolution of subcontinental mantle.
884 Geochimica et Cosmochimica Acta 53, 1583-1595.

885 Weaver, B.L. (1991) The origin of ocean island basalt end-member compositions: trace element and isotopic
886 constraints. Earth and Planetary Science Letters 104, 381-397.

887 Weaver, S.D., Storey, B.C., Pankhurst, R.J., Mukasa, S.B., DiVenere, V.J. and Bradshaw, J.D. (1994)
888 Antarctica-New Zealand rifting and Marie Byrd Land lithospheric magmatism linked to ridge subduction and
889 mantle plume activity. Geology 22, 811-814.

890 Winberry, J.P. and Anandakrishnan, S. (2004) Crustal structure of the West Antarctic rift system and Marie Byrd
891 Land hotspot. Geology 32, 977-980.

892 Witt-Eickschen, G., Seck, H.A., Mezger, K., Eggins, S.M. and Altherr, R. (2003) Lithospheric mantle evolution
893 beneath the Eifel (Germany): Constraints from Sr–Nd–Pb isotopes and trace element abundances in spinel
894 peridotite and pyroxenite xenoliths. Journal of Petrology 44, 1077-1095.

Wittig, N., Pearson, D.G., Downes, H. and Baker, J.A. (2009) The U, Th and Pb elemental and isotope compositions of mantle clinopyroxenes and their grain boundary contamination derived from leaching and digestion experiments. Geochimica et Cosmochimica Acta 73, 469-488.

Wittig, N., Pearson, D.G., Duggen, S., Baker, J.A. and Hoernle, K. (2010) Tracing the metasomatic and magmatic evolution of continental mantle roots with Sr, Nd, Hf and and Pb isotopes: A case study of Middle Atlas (Morocco) peridotite xenoliths. Geochimica et Cosmochimica Acta 74, 1417-1435.

Wolley, A.R. and Bailey, D.K. (2012) The crucial role of lithospheric structure in the generation and release of carbonatites: geological evidence. Mineralogical Magazine 76, 259-270.

Woodhead, J.D. (1996) Extreme HIMU in an oceanic setting: the geochemistry of Mangaia Island (Polynesia), and temporal evolution of the Cook-Austral hotspot. Journal of Volcanology and Geothermal Research 72, 1-19.

Workman, R.K. and Hart, S.R. (2005) Major and trace element composition of the depleted MORB mantle (DMM). Earth and Planetary Science Letters 231, 53-72.

Zhang, M. and O'Reilly, S.Y. (1997) Multiple sources for basaltic rocks from Dubbo, eastern Australia: geochemical evidence for plume—lithospheric mantle interaction. Chemical Geology 136, 33-54.

Zhang, M., Stephenson, P.J., O'Reilly, S., McCulloch, M.T. and Norman, M.D. (2001) Petrogenesis and geodynamic implications of Late Cenozoic basalts in North Queensland, Australia: Trace-element and Sr–Nd–Pb isotope evidence. Journal of Petrology 42, 685-719.

Zindler, A. and Hart, S.R. (1986) Chemical geodynamics. Annual Reviews of Earth and Planetary Science 14, 493-571.

915 **Figure Captions**

916 *Figure 1*: Simplified geological map of New Zealand's crustal basement showing the mantle
917 xenolith localities. Crustal geology is based on Mortimer (2004). Mantle xenoliths are divided
918 into three groups: (1) Waitaha domain (circles); Chatham Islands (squares); and (3) all other
919 localities (diamonds) based on Re-Os isotopic characteristics (McCoy-West *et al.*, 2013). The
920 dashed ellipse represents the minimum extent of the Paleoproterozoic Waitaha domain of
921 lithospheric mantle. Previously studied xenolith localities are shown divided as follows; those
922 considered to be within the Waitaha domain (black circles; Scott et al., 2014b), the Auckland
923 Islands (blue square) and West Otago (grey diamonds; Liu et al., 2015).
924
925 *Figure 2:* Comparison of concentrations and ratios of trace elements in unleached
926 clinopyroxene measured by laser ablation (McCoy-West et al., 2015) and clinopyroxene
927 residues after leaching analysed by TIMS. (a-b) concentrations of Sr and Pb, respectively. (c-
928 f) Sm/Nd, Th/U, U/Pb and Th/Pb ratios, respectively. Samples with any element with a
929 concentration measured by laser of <15 ppb are shown white. The leachates of the high
930 concentration sample DPP-1 as measured by TIMS have isotopic ratios (e.g. Th/U) far from
931 unity, whereas the leached residue of this sample plots on the 1:1 line.
932
933 *Figure 3*: Comparison of (a) $^{87}Sr/^{86}Sr$ versus $^{87}Rb/^{86}Sr$ and (b) $^{143}Nd/^{144}Nd$ versus $^{147}Sm/^{144}Nd$
934 isotopic systematics of mantle xenoliths from around Zealandia. Mantle xenoliths are divided
935 into three groups: (1) Waitaha domain (circles); Chatham Islands (squares); and (3) all other
936 localities (triangles) based on Re-Os isotopic characteristics (McCoy-West et al., 2013). (a)
937 The Waitaha domain exhibits greater isotopic heterogeneity, with no simple correlation
938 observed between $^{87}Rb/^{86}Sr$ and $^{87}Sr/^{86}Sr$. (b) Several arrays appear to form in Sm-Nd isotopic
939 space, consistent with at least two events; Paleoproterozoic and Cretaceous melting with the
940 remainder probably being mixed ages. Comparative xenolith data (Scott et al., 2014a; 2014b)
941 are separated into samples considered to be within the Waitaha domain (North and East
942 Otago; black circles; n = 28), and those from the Auckland Islands (blue squares; n = 4).
943
944 *Figure 4:* Strontium-Nd-Pb isotopic plots comparing Zealandian mantle xenoliths to oceanic
945 mantle end-member compositions and intraplate basalts from the New Zealand region. Whole
946 rock analyses (triangles) and clinopyroxene separates (squares) are distinguished. Error bars
947 are generally significantly smaller than the size of the symbols, except where shown Pb

948 analyses. Data sources for mantle end-member compositions are provided in Fig. EA4. The
949 archetypal example of HIMU end-member from the Cook-Austral Islands, Mangaia is shown
950 separately (Woodhead, 1996). New Zealand intraplate basalts have been divided into two
951 groups on the basis of their location, the North Island (Cook et al., 2005; Huang et al., 2000;
952 Huang et al., 1997; McGee et al., 2013; Sprung et al., 2007; Timm et al., 2010) and southern
953 Zealandia (i.e. the South Island and all the outlying Islands on the Campbell Plateau; Barreiro
954 and Cooper, 1987; Hoernle et al., 2006; McCoy-West et al., 2010; Panter et al., 2006; Sprung
955 et al., 2007; Timm et al., 2009; Timm et al., 2010), with samples showing evidence of crustal
956 contamination excluded (i.e. consistent with assimilation of Torlesse Greywacke: SiO_2 >52 wt
957 % or $^{87}Sr/^{86}Sr$ >0.7038; McCoy-West et al., 2010). NRHL = northern hemisphere reference
958 line: Hart (1984). Mantle xenoliths are compared to mantle components uncorrected for the
959 host basalt eruption age, this correction makes negligible difference to the majority of Sr-Nd
960 data, and has minimal effect on Pb data for the majority of samples due to the young eruption
961 ages (<86 Ma), and is only significant for those samples with extremely elevated $^{238}U/^{204}Pb$
962 >100 (see Fig. EA4).
963
964 *Figure 5*: Lithophile isotope (Sr-Nd and Pb) variation of Zealandian mantle xenoliths relative
965 to their degree of metasomatism (i.e. whole rock La/Yb_N; N = chondrite-normalised; Palme &
966 O'Neill, 2014). Unmetasomatised samples (La/Yb_N <1) from the Waitaha domain possess the
967 greatest isotopic heterogeneity. As the degree of metasomatism increases Sr and Nd isotopic
968 compositions converge to that of the metasomatic agent (e.g. grey bar; $^{87}Sr/^{86}Sr$ = 0.7028-
969 0.7033; ε_{Nd} = +3-+6), while Pb isotopic compositions remain more heterogeneous ($^{206}Pb/^{204}Pb$
970 = 19.5-21). Comparative xenolith data (Scott et al., 2014a; 2014b) has been plotted using the
971 La/Yb_N of clinopyroxene. Also shown are Alpine Dyke Swarm carbonatites (La/Yb_N >>25;
972 Barreiro and Cooper, 1987) and oceanic carbonatites unaffected by crustal contamination
973 from Fogo and Brava, Cape Verde Islands (Hoernle et al., 2002; Mourão et al., 2012).
974
975 *Figure 6*: Comparison of Pb isotopic compositions of Zealandian mantle xenoliths with other
976 isotopic data. The shaded bar represents a restricted range of Pb isotopic compositions
977 ($^{206}Pb/^{204}Pb$ = 19.5-20.5; $^{208}Pb/^{204}Pb$ = 39-40) to illustrate the lack of correlation between Pb
978 isotopic ratios and parent-daughter ratios (a-b) or other isotopic systems (Nd and Os; c-d). (a-
979 b) the dotted lines show the range of $^{238}U/^{204}Pb$ and $^{232}Th/^{204}Pb$ required to explain the
980 variability observed in the HIMU end-member based on 0.5-3.0 Ga old recycled oceanic crust

($^{238}U/^{204}Pb$ = 12-61; $^{232}Th/^{204}Pb$ = 45-177; Stracke et al., 2003). Mangaia represents the archetypal example of the classical HIMU end-member (Woodhead, 1996), with peridotite xenoliths from the Atlas Mountains, Morocco also shown (Wittig et al., 2010). (d) the $^{187}Os/^{186}Os$ isotopic composition of the PUM (primitive upper mantle) is 0.1296 ± 8 (Meisel et al., 2001) with the age scale showing the approximate Re-depletion model ages based on these compositions.

Figure 7: (a) Histogram showing average ^{206}Pb and ^{208}Pb T_{Meta} metasomatic model ages for xenoliths from the Waitaha domain and Chatham Islands. Relative probability curves, assuming a 20 Ma error on the ages, are shown for ^{238}U-^{206}Pb (solid line) and ^{232}Th-^{208}Pb (dotted line) metasomatic ages (see Table 2). (b) Plot of eruption age of the host basalt versus the average metasomatic model ages of mantle xenoliths. Also shown are the errorchron ages for individual localities (see Table 3). The filled box plot represents the weighted average of the preferred errorchrons and a 95% confidence interval error, with the dotted line representing the all-inclusive 95% confidence interval error. Ages of geologic events are taken from Eagles et al. (2004); Hoernle et al. (2010); Kamp (1986); McCoy-West et al. (2010).

Figure 8: ^{238}U-$^{206}Pb$and ^{232}Th-^{208}Pb errorchrons of mantle xenoliths from individual localities within Zealandia, the Chatham Islands (a-b), Fortification Peak (c-d), Pilot Point (e-f) and Trig L (g-h). These ages are only considered indicative of the timing of metasomatism and assume the samples were initially in isotopic equilibrium. However, they demonstrate how quickly ingrowth of these radiogenic Pb signatures can occur with such extreme parent-daughter ratios. Errorchron ages are preferred ages (solid lines; see Table 3). Samples plotted white are excluded from the age calculations with the grey ages and dotted lines showing the effect of including these samples.

Figure 9: Unique Pb isotopic characteristics of Zealandian xenoliths due to metasomatism: (a) $^{238}U/^{204}Pb$ versus Δ7/4; and (b) Nb/Ta of clinopyroxene crystals versus Δ7/4. Hollow symbols represent individual crystal analyses, with the filled symbols showing the average value for the xenolith. Δ7/4 is the vertical deviation in $^{207}Pb/^{204}Pb$ calculated relative to the northern hemisphere reference line (Hart, 1984). The majority of samples are strongly metasomatised and have Pb isotopic compositions similar to Cape Verde carbonatites

(Hoernle et al., 2002; Mourão et al., 2012) and Atlas mountains xenoliths (Wittig et al., 2009; Wittig et al., 2010) whereas, weakly metasomatised samples have not equilibrated with the metasomatic agent and preserve strongly negative Δ7/4 coupled with extreme $^{238}U/^{204}Pb$ and Nb/Ta fractionations consistent with carbonatite metasomatism.

Figure 10: Modelled Pb isotopic compositions of mantle xenoliths from the Waitaha domain 200 m.y. in the future. White symbols represent the present day measured compositions; with filled colour symbols representing the modelled isotopic compositions (see Table EA5). The blue circles joined by dotted lines represent the evolution of three distinct samples in 50 m.y. intervals. The five samples with the most extreme $^{238}U/^{204}Pb$ already plot significantly off the graph (see Table EA5). The evolution of Mangaia, the archetypal example of the HIMU end-member (Woodhead, 1996), and Atlas Mountain xenoliths (Wittig et al., 2010), over the same time interval are shown for comparison. The variability of U/Pb, Th/Pb and Th/U within the xenoliths will result in the rapid development of highly radiogenic and heterogeneous Pb isotope signature in the future, with compositions different from any known mantle reservoirs.

Figure 11: Schematic diagram showing the complex history of the lithospheric mantle under Zealandia during the Phanerozoic. The nascent lithosphere of the Waitaha domain formed at ca. 1.9 Ga on the margin of the Paleoproterozoic supercontinent Nuna, subsequently the Waitaha domain SCLM became partially or totally decoupled from its complementary overlying crust and remained isolated from other major crustal bodies without being significantly reworked for >1 G.y. (McCoy-West et al., 2013). (a) The Waitaha domain arrived at the eastern margin of Gondwana after ca. 280 Ma (Kimbrough et al., 1992), because of its present day position to the east of the Dun Mountain Ophiolite Belt, preserving evidence of a major oceanic basin closure event. (b) Carbonate-rich low degree melts in a weak mantle upwelling, possibly in the form of a mantle plume, heterogeneously metasomatised the SCLM imparting a distinctive elevated U/Pb and Th/Pb signature (CarboHIMU). This event is interpreted to occur in the Early Cretaceous, ca. 120-110 Ma, based on melting and metasomatic ages (see Figs. 7; 8; EA5). (c) Sea-floor spreading between Zealandia and Marie Byrd Land, West Antarctica, is constrained at ca. 84 Ma by the oldest oceanic crust adjacent to the Campbell Plateau (Eagles et al., 2004). (d) Over the last 84 Ma alkaline intraplate volcanism has been ongoing while Zealandia has drifted 6000 km northwest (Timm et al., 2010). These melts have continuously reactivated the metasomatic signature producing the

young metasomatic ages observed (Fig. 8). Arrows represent the direction and relative strength of mantle flow.

Table Footnotes

Table 1:

[A]Sample type: [1] whole rock powder; [2] clinopyroxene separate; [3] orthopyroxene separate. # is a replicate digestion of the sample. Replicate digestions of sample FvF-1 contained [c] coarse (425-500 µm) and [f] fine (275-425 µm) clinopyroxene.

[B]Whole rock Al_2O_3 contents from McCoy-West et al. (2015).

[C]Whole rock La/Yb_N (chondrite-normalised; Palme and O'Neill, 2014) ratios are calculated from data in McCoy-West et al. (2015). *For samples from the Pilot Point locality clinopyroxene ratios were used as whole rock compositions are disturbed by alteration (McCoy-West et al., 2015).

[D]Initial $^{187}Os/^{188}Os$ is taken from McCoy-West et al. (2013).

[E]Initial isotopic compositions are calculated using the age of eruption of the host basalt at each locality, which can be found in (McCoy-West et al., 2015).

[F] $\varepsilon_{Nd}(T) = (((^{143}Nd/^{144}Nd_{sam}(T) / {}^{143}Nd/^{144}Nd_{CHUR}(T)) -1) \times 10^4$ where T is the age of eruption of the host basalt and is calculated using the CHUR compositions below.

[G]Nd model ages are only shown for those samples that have been weakly metasomatised (i.e. $La/Yb_N < 1$). T_{CHUR} was calculated assuming $^{147}Sm/^{144}Nd = 0.1967$ and $^{143}Nd/^{144}Nd = 0.512638$ (Jacobsen and Wasserburg, 1984). T_{DM} was calculated assuming $^{147}Sm/^{144}Nd = 0.2136$ and $^{143}Nd/^{144}Nd = 0.51315$, the depleted MORB mantle composition of Workman and Hart (2005).

Sr, Sm and Nd concentration data are precise to better than 0.02 %, 0.05 % and 0.05 %, respectively. Rb concentrations are generally precise to 0.2-0.4 %, although rare samples with the lowest concentrations have up to a 2.5 % error.

Table 2:

[A]Sample type: [1] whole rock powder; [2] clinopyroxene separate; [3] orthopyroxene separate. # is a replicate digestion of the sample. Replicate digestions of sample FvF-1 contained [c] coarse (425-500 µm) and [f] fine (275-425 µm) clinopyroxene.

[B]Initial Pb isotopic compositions are calculated using the age of eruption of the host basalt at each locality, which can be found in McCoy-West et al. (2015).

[C]$\Delta 7/4$ and $\Delta 8/4$ are the vertical deviation in $^{207}Pb/^{204}Pb$ and $^{208}Pb/^{204}Pb$ calculated relative to the northern hemisphere reference line (Hart, 1984).

[D]T_{Meta}^{206} and T_{Meta}^{208} provide an estimate of how long it would take to evolve the measured $^{206}Pb/^{204}Pb$ and $^{208}Pb/^{204}Pb$ ratios, respectively, in the samples assuming that metasomatism created their elevated U/Pb and Th/Pb ratios and their original isotopic composition were that of unmetasomatised sample OU45852 ($^{206}Pb/^{204}Pb = 19.568$; $^{208}Pb/^{204}Pb = 39.056$).

U, Th and Pb concentration data are generally precise to better than 0.1 %, 0.3 % and 0.001%, respectively.

Table 3:

Errorchron age estimates were calculated using isoplot (Ludwig, 2008), using either the measured errors or a 1% error on the parent daughter ratio (whichever was larger), and the reproducibility of Pb standard isotope measurements over a 2 year period (2σ population: $^{206}Pb/^{204}Pb = \pm 0.018$; $^{207}Pb/^{204}Pb = \pm 0.013$; $^{208}Pb/^{204}Pb = \pm 0.055$). Weighted averages are calculated using the three linked decay schemes.

[A] The assumption underpinning the errorchrons is that the samples were in isotopic equilibrium prior to the addition of the metasomatic agent. All-inclusive ages are based on data from all samples analysed for a given locality. Preferred ages exclude any samples were the assumption of prior equilibrium clearly does not hold (i.e. data points are greater than 3x

1101 the external Pb reproducibility, e.g. = ± 0.054 (2σ) for $^{206}Pb/^{204}Pb$, from the regression formed
1102 by the other points).
1103 [B] n = the number of samples included in a calculation. Numbers in parentheses represent the
1104 total number of xenoliths analysed at a locality.
1105 [C] Reasons for exclusion: Chatham Islands; Clinopyroxene separates were the smallest
1106 measured in this study (<10 mg) and preserve heterogeneity unrelated to the metasomatism.
1107 Fortification Peak; Sample WFP-8 falls below the regression line consistent with being a
1108 Paleoproterozoic melt residue (ε_{Nd} >+27) that preserves an unradiogenic Pb composition that
1109 has not equilibrated with the metasomatic agent. Pilot Point; the small whole rock xenoliths
1110 do not preserve evidence of the unradiogenic Pb composition seen in the clinopyroxene
1111 separates. MSWD >> 1000 suggests that this is not a single population. Trig L; Sample
1112 WTL-3 is excluded due to its significant offset in $^{206}Pb/^{204}Pb$ from the other xenoliths in this
1113 overall weakly metasomatised locality (McCoy-West et al., 2015).
1114

Table 1: Rb-Sr and Sm-Nd concentration and isotopic data for whole rocks and mineral separates from New Zealand mantle xenoliths.

Sample [A]	Al_2O_3 [B] (wt %)	La/Yb_N [C]	$^{187}Os/^{188}Os_{(i)}$ [D]	Rb (ppm)	Sr (ppm)	$^{87}Rb/^{86}Sr$	$^{87}Sr/^{86}Sr$ [E] measured	$^{87}Sr/^{86}Sr$ [E] initial	Sm (ppm)	Nd (ppm)	$^{147}Sm/^{144}Nd$	$^{143}Nd/^{144}Nd$ [E] measured	$^{143}Nd/^{144}Nd$ [E] initial	ε_{Nd} [F]	T_{CHUR} (Ga) [G]	T_{DM} (Ga) [G]
North Island																
NGB-3[1]	0.06	2.76	0.12700	0.0347	4.583	0.0219	0.703532 ±12	0.70353	0.0200	0.0072	0.2163	0.513029 ±12	0.51303	7.6 ±2	--	--
NGB-4[1]	0.16	29.8	0.12942	0.1159	4.691	0.0714	0.703183 ±9	0.70318	0.0881	0.0169	0.1158	0.512953 ±7	0.51295	6.2 ±1	--	--
South Island																
P43153b[1]	1.02	9.48	0.11242	0.5356	3.022	0.5128	0.709371 ±5	0.70878	0.0987	0.0224	0.1373	0.512895 ±5	0.51282	5.0 ±1	--	--
P45280[1]	0.53	0.873	0.12584	0.0554	0.383	0.4184	0.703340 ±8	0.70282	0.0534	0.0197	0.2228	0.512952 ±8	0.51282	6.1 ±2	1.83	-3.34
MSI33D[1]	0.71	8.84	0.12406	0.6785	6.696	0.2930	0.703061 ±5	0.70295	0.5962	0.1709	0.1733	0.512869 ±3	0.51284	4.5 ±1	--	--
MSIK33C[1]	1.73	4.81	0.12630	0.0648	2.789	0.0672	0.703448 ±8	0.70342	0.3641	0.1209	0.2008	0.512872 ±8	0.51284	4.6 ±2	--	--
Waitaha domain																
MSI20C[2]	1.26	16.54	0.11982	0.0193	67.84	0.0008	0.702850 ±5	0.70285	2.165	0.2869	0.0801	0.512950 ±6	0.51295	6.1 ±1	--	--
MSI20G[1]	1.62	15.22	0.11989	0.0228	2.768	0.0238	0.702966 ±7	0.70296	0.1123	0.0190	0.1022	0.512926 ±16	0.51292	5.6 ±3	--	--
MSI20G[1]#									0.0940	0.0155	0.1000	0.512928 ±12	0.51292	5.7 ±2	--	--
FvF-1[2c]	2.61	0.888		0.3471	33.41	0.0300	0.702645 ±9	0.70264	1.649	0.6333	0.2323	0.513469 ±8	0.51342	16.2 ±2	3.53	2.59
FvF-1[2f]				0.4536	36.31	0.0361	0.702639 ±7	0.70263	1.757	0.6380	0.2196	0.513430 ±8	0.51339	15.4 ±2	--	--
MSI79C[1]	3.45	1.59	0.11953	0.0574	7.174	0.0231	0.703162 ±8	0.70315	0.2721	0.0973	0.2163	0.513599 ±8	0.51355	18.7 ±2	--	--
WTL-1[2]	2.64	0.528	0.12390	0.0204	4.977	0.0118	0.702564 ±8	0.70256	0.5154	0.4348	0.5101	0.512969 ±6	0.51291	6.5 ±1	0.16	-0.09
WTL-2[2]	1.45	22.2	0.11703	0.0250	26.43	0.0027	0.703186 ±6	0.70318	0.5977	0.3621	0.3664	0.513792 ±4	0.51375	22.5 ±1	--	--
WTL-3[2]	2.02	0.473	0.12152	0.0054	0.372	0.0417	0.702766 ±28	0.70275	0.4002	0.5571	0.8418	0.513203 ±6	0.51310	11.0 ±1	0.13	0.01
OU45852[1]	2.35	0.172	0.12380	0.0048	0.221	0.0631	0.704426 ±10	0.70441	0.0416	0.0453	0.6580	0.513785 ±9	0.51370	22.4 ±2	0.38	0.22
OU45852[2]				0.0038	0.876	0.0127	0.702057 ±11	0.70205	0.3783	0.4270	0.6826	0.513839 ±11	0.51376	23.4 ±2	0.38	0.22
OU45852[2]#				0.0053	1.034	0.0147	0.702061 ±8	0.70206	0.4019	0.4392	0.6607	0.513788 ±74	0.51371	22.4 ±14	0.38	0.22
WRR-1[2]	1.44	4.93	0.11662	0.0037	4.853	0.0022	0.703555 ±5	0.70356	5.101	1.445	0.1714	0.512850 ±8	0.51283	4.1 ±2	--	--
WRR-5[2]	0.76	9.93	0.11797	0.0220	43.75	0.0015	0.702786 ±10	0.70279	2.860	0.0145	0.0031	0.512841 ±6	0.51284	4.0 ±1	--	--
WRR-7[2]	1.00	6.77	0.11653	0.0182	19.69	0.0027	0.703168 ±9	0.70317	2.274	0.5986	0.1592	0.512993 ±7	0.51298	6.9 ±1	--	--
WRR-9[3]	1.06	21.0	0.11764	1.392	7.444	0.5407	0.702975 ±7	0.70285	0.4856	0.0860	0.1071	0.512933 ±17	0.51292	5.7 ±3	--	--
DPP-1[2]		0.562*		0.0903	21.43	0.0122	0.701973 ±8	0.70197	1.786	1.020	0.3454	0.513751 ±14	0.51372	21.7 ±3	1.14	0.70
DPP-1[2]#				0.2013	19.84	0.0293	0.701971 ±7	0.70197	1.723	0.9721	0.3412	0.513659 ±34	0.51363	19.9 ±7	1.08	0.61
DPP-2[1]	1.34	22.8*	0.11559	0.3567	5.706	0.1808	0.703029 ±6	0.70299	0.2490	0.0522	0.1268	0.512865 ±8	0.51285	4.4 ±2	--	--
DPP-3[2]	3.24	0.270*		0.0168	57.99	0.0008	0.702466±10	0.70247	3.464	1.455	0.2585	0.513412 ±5	0.51339	15.1 ±1	1.90	0.89
DPP-3[2]#				0.0235	57.50	0.0012	0.702464 ±7	0.70246	3.404	1.479	0.2582	0.513414 ±7	0.51339	15.1 ±1	1.92	0.90

Sample [A]	Al_2O_3 [B] (wt %)	La/Yb_N [C]	$^{187}Os/^{188}Os_{(i)}$ [D]	Rb (ppm)	Sr (ppm)	$^{87}Rb/^{86}Sr$	$^{87}Sr/^{86}Sr$ [E] measured	$^{87}Sr/^{86}Sr$ [E] initial	Sm (ppm)	Nd (ppm)	$^{147}Sm/^{144}Nd$	$^{143}Nd/^{144}Nd$ [E] measured	$^{143}Nd/^{144}Nd$ [E] initial	ε_{Nd} [F]	T_{CHUR} (Ga) [G]	T_{DM} (Ga) [G]
DPP-5[2]		0.043*		0.1632	18.18	0.0260	0.702112 ±9	0.70211	2.088	1.157	0.3351	0.513393 ±8	0.51336	14.7 ±2	0.83	0.31
DPP-5[2]#				0.2320	19.09	0.0351	0.702076 ±5	0.70207	2.083	1.170	0.3397	0.513386 ±14	0.51336	14.6 ±3	0.80	0.29
DPP-6[1]	3.87	0.945*	0.12566	0.4554	7.389	0.1782	0.702818±7	0.70279	0.5864	0.1978	0.2040	0.512918 ±4	0.51290	5.5 ±7	--	--
WFP-1[2]	0.98	10.8	0.13293	0.2501	120.0	0.0060	0.702725 ±3	0.70272	1.230	0.2151	0.1058	0.512894 ±9	0.51288	5.0 ±2	--	--
WFP-2[2]	1.96	0.762	0.12684	0.0204	20.45	0.0029	0.702811 ±4	0.70281	1.750	0.6860	0.2371	0.513037 ±5	0.51301	7.8 ±9	1.50	-0.73
WFP-4[2]	0.56	7.09		0.0256	11.78	0.0063	0.703213 ±10	0.70321	1.335	0.2487	0.1126	0.512797 ±6	0.51279	3.1 ±1	--	--
WFP-4[2]#				0.0223	13.45	0.0048	0.703173 ±7	0.70317	1.528	0.2921	0.1156	0.512805 ±6	0.51279	3.2 ±1	--	--
WFP-5[2]	0.81	3.64		0.4626	15.26	0.0877	0.703046 ±8	0.70303	1.067	0.2955	0.1675	0.512804 ±6	0.51279	3.2 ±1	--	--
WFP-8[2]	1.89	0.328	0.12354	0.0346	0.561	0.1783	0.704153 ±19	0.70411	0.0418	0.0189	0.2732	0.514014 ±46	0.513987	26.9 ±9	2.73	2.20
WFP-8[2]#				0.0444	0.603	0.2133	0.704202 ±17	0.70416	0.0407	0.0191	0.2836	0.514226 ±19	0.51420	31.0 ±3	2.77	2.33
WFP-11[1]	0.54	14.5	0.12573	0.3884	1.524	0.7371	0.702916 ±7	0.70292	0.1320	0.0277	0.1269	0.512879 ±9	0.51287	4.7 ±2	--	--
WFP-11[2]				0.3947	73.66	0.0155	0.702680 ±7	0.70268	4.737	0.9747	0.1244	0.512856 ±11	0.51284	4.2 ±2	--	--
Chatham Islands																
P80180[2]	0.78	14.3	0.12408	1.8972	284.1	0.0193	0.702925 ±9	0.70290	34.04	7.837	0.1392	0.512829 ±4	0.51275	3.7 ±8	--	--
P80290[1]	0.57	20.0		0.1991	5.471	0.1052	0.703025 ±5	0.70290	0.1342	0.0279	0.1256	0.512816 ±6	0.51275	3.5 ±1	--	--
P80291[2]	0.64	23.2	0.12989	0.7867	341.1	0.0067	0.702902 ±6	0.70289	27.49	5.601	0.1232	0.512815 ±9	0.51275	3.5 ±2	--	--
P80354a[1]	0.61	9.01		0.0659	2.510	0.0759	0.703014 ±5	0.70295	0.1034	0.0292	0.1706	0.512836 ±15	0.51277	3.9 ±3	--	--
P80354b[1]	0.51	4.59	0.12169	0.0865	1.471	0.1702	0.703187 ±5	0.70304	0.0926	0.0280	0.1829	0.512862 ±17	0.51279	4.4 ±3	--	--
P80354c[1]	0.74	2.94	0.12163	0.0698	4.047	0.0499	0.702875 ±4	0.70283	0.6535	0.195	0.1806	0.512843 ±5	0.51277	4.0 ±1	--	--

Table 2: U-Th-Pb concentration and isotopic data from New Zealand mantle xenoliths.

Sample [A]	U (ppm)	Th (ppm)	Pb (ppm)	$^{238}U/^{204}Pb$	$^{235}U/^{204}Pb$	$^{232}Th/^{204}Pb$	$^{206}Pb/^{204}Pb$ [B] measured	initial	$^{207}Pb/^{204}Pb$ [B] measured	initial	$^{208}Pb/^{204}Pb$ [B] measured	initial	Δ7/4 [C]	Δ8/4 [C]	T_{Meta}^{206} (Ma) [D]	T_{Meta}^{208} (Ma) [D]
North Island																
NGB3[1]	0.0009	0.0017	0.0284	1.99	0.014	3.95	18.681 ± 6	18.68	15.5853 ± 57	15.59	38.461 ± 15	38.46	6.93	25.0		
NGB4[1]	0.0289	0.1308	0.0290	63.2	0.458	291.1	18.638 ± 2	18.62	15.5575 ± 22	15.56	38.2950 ± 60	38.27	4.62	13.5		
South Island																
P43153b[1]	0.0111	0.0155	0.0223	32.0	0.232	45.4	19.55 ± 10	19.15	15.463 ± 96	15.44	38.33 ± 31	38.15	-14.7	-93.1		
P45280[1]	0.0004	0.0013	0.0144	1.92	0.014	6.01	19.000 ± 7	18.97	15.6358 ± 61	15.64	38.81 ± 16	38.79	8.52	21.8		
MSI33D[1]	0.0105	0.0352	0.0295	23.6	0.171	80.1	20.063 ± 5	19.97	15.6694 ± 35	15.66	39.6731 ± 94	39.57	0.35	-21.0		
MSIK33C[1]	0.0062	0.0154	0.0083	48.8	0.354	123.1	19.839 ± 11	19.64	15.7051 ± 68	15.70	39.217 ± 21	39.06	6.36	-39.5		
Waitaha domain																
MSI20C[2]	0.4589	1.6653	0.4785	63.1	0.458	232.9	19.909 ± 2	19.83	15.6247 ± 9	15.621	39.6110 ± 37	39.51	-2.44	-8.55	34.7	48.1
MSI20G[1]	0.0186	0.0660	0.0166	73.5	0.533	266.0	19.937 ± 10	19.84	15.6381 ± 68	15.634	39.603 ± 19	39.49	-1.41	-12.8	32.3	41.5
FvF-1[2c]	0.0544	0.1910	0.0382	93.7	0.680	334.7	20.015 ± 8	19.75	15.6205 ± 44	15.608	39.435 ± 13	39.14	-4.02	-39.1	30.7	22.8
FvF-1[2f]	0.0548	0.1940	0.0428	84.1	0.610	303.3	20.006 ± 7	19.77	15.6242 ± 50	15.613	39.433 ± 14	39.16	-3.55	-38.1	33.5	25.1
MSI79C[1]	0.0095	0.0334	0.0132	47.5	0.345	169.9	20.150 ± 13	19.90	15.6523 ± 85	15.641	39.457 ± 23	39.17	-2.30	-53.1	78.5	47.6
WTL-1[2]	0.0005	0.0003	0.0441	0.69	0.005	0.52	19.687 ± 4	19.69	15.6156 ± 23	15.616	39.1155 ± 70	39.12	-0.95	-31.4	--	--
WTL-2[2]	0.1129	0.1470	0.0642	115.5	0.838	153.0	20.121 ± 6	19.79	15.6405 ± 27	15.625	39.3013 ± 91	39.16	-3.16	-65.2	30.8	32.3
WTL-3[2]	0.0004	0.0026	0.0009	31.6	0.229	190.9	21.13 ± 23	21.04	15.6334 ± 725	15.63	39.40 ± 24	39.23	-14.8	-176.9	311	36.7
OU45852[1]	0.0003	0.0019	0.0065	2.58	0.019	19.1	19.679 ± 8	19.67	15.6144 ± 52	15.61	39.165 ± 19	39.15	-0.99	-25.4	--	--
OU45852[1]#	0.0002	0.0004	0.0026	5.33	0.039	10.1	19.760 ± 26	19.75	15.5962 ± 197	15.60	39.208 ± 52	39.20	-3.68	-30.9	--	--
OU45852[2]	0.0004	0.0014	0.0116	2.44	0.018	8.24	19.568 ± 10	19.56	15.6089 ± 48	15.61	39.056 ± 17	39.05	-0.33	-22.8	--	--
WRR-1[2]	0.1640	0.6070	0.1205	90.4	0.656	340.6	20.252 ± 2	20.02	15.6701 ± 10	15.66	39.9903 ± 34	39.71	-1.62	-12.1	48.6	55.3
WRR-5[2]	0.3213	0.3081	0.2638	80.8	0.586	78.8	20.384 ± 5	20.18	15.6666 ± 44	15.66	39.688 ± 14	39.62	-3.40	-58.3	64.8	161
WRR-7[2]	0.1633	0.3748	0.1207	89.4	0.648	208.6	20.176 ± 4	19.95	15.6518 ± 24	15.64	39.5720 ± 70	39.40	-2.63	-44.8	43.8	49.9
WRR-9[3]	0.1140	0.3969	0.2986	25.2	0.183	89.2	20.122 ± 2	20.06	15.6583 ± 18	15.66	39.5315 ± 58	39.46	-1.39	-42.3	140	107
DPP-1[2]	0.2104	0.9960	0.0257	552.2	4.00	2659	20.699 ± 47	19.59	15.5809 ± 335	15.53	40.648 ± 91	38.94	-15.4	-0.47	13.2	12.1
DPP-1[2]#	0.1990	1.0485	0.0288	466.2	3.38	2499	20.693 ± 9	19.75	15.6396 ± 60	15.60	40.635 ± 17	39.03	-9.45	-0.95	15.5	12.8
DPP-2[1]	0.0129	0.0224	0.0115	74.4	0.540	130.8	20.068 ± 13	19.92	15.6463 ± 70	15.64	39.510 ± 23	39.43	-2.00	-37.9	43.2	70.0
DPP-3[2]	0.0057	0.0180	0.0414	8.39	0.061	26.9	17.260 ± 8	17.24	15.3692 ± 56	15.37	36.867 ± 15	36.85	0.72	37.6	--	--

Sample [A]	U (ppm)	Th (ppm)	Pb (ppm)	$^{238}U/^{204}Pb$	$^{235}U/^{204}Pb$	$^{232}Th/^{204}Pb$	$^{206}Pb/^{204}Pb$ [B]		$^{207}Pb/^{204}Pb$ [B]		$^{208}Pb/^{204}Pb$ [B]		$\Delta 7/4$ [C]	$\Delta 8/4$ [C]	T_{Meta}^{206} (Ma) [D]	T_{Meta}^{208} (Ma) [D]
							measured	initial	measured	initial	measured	initial				
DPP-3[2]#	0.0066	0.0202	0.0431	9.44	0.068	29.2	17.469 ± 5	17.45	15.3662 ± 40	15.37	37.078 ± 11	37.06	-1.84	33.1	--	--
DPP-5[2]	0.0049	0.0119	0.0027	113.4	0.822	280.7	18.00 ± 24	17.77	15.36 ± 20	15.36	37.42 ± 49	37.24			--	--
DPP-5[2]#	0.0054	0.0131	0.0029	114.8	0.833	284.3	18.443 ± 25	18.21	15.358 ± 20	15.35	37.664 ± 52	37.48	-13.2	-26.1	--	--
DPP-6[1]	0.0187	0.0594	0.0237	52.5	0.380	169.6	20.380 ± 7	20.27	15.6794 ± 41	15.67	39.816 ± 12	39.71	-2.08	-45.1	99.0	90.3
WFP-1[2]	0.4092	1.9719	0.0670	472.9	3.43	2318	25.420 ± 17	24.28	15.9347 ± 39	15.88	47.278 ± 26	45.50	-31.2	91.8	79.3	71.5
WFP-2[2]	0.0156	0.0650	0.0588	17.6	0.127	74.2	20.157 ± 7	20.11	15.6769 ± 39	15.68	39.618 ± 13	39.56	0.09	-37.8	212	152
WFP-4[2]	0.1187	0.2735	0.1178	67.2	0.487	157.6	20.598 ± 4	20.43	15.6815 ± 22	15.67	39.9391 ± 69	39.82	-4.19	-58.6	97.7	113
WFP-5[2]	0.0242	0.0684	0.0186	88.1	0.639	252.8	21.008 ± 21	20.80	15.6948 ± 66	15.69	40.588 ± 30	40.39	-7.35	-43.8	105	122
WFP-8[2]	0.0079	0.0205	0.0015	356.7	2.59	944.7	21.34 ± 10	20.48	15.684 ± 39	15.65	40.42 ± 14	39.70	-11.9	-100.2	31.9	29.1
WFP-11[1]	0.0081	0.0250	0.0217	24.6	0.178	77.6	20.436 ± 7	20.38	15.6939 ± 47	15.69	39.763 ± 14	39.70	-1.24	-57.2	224	183
WFP-11[2]	0.0184	0.0565	0.0869	14.2	0.103	44.1	20.585 ± 28	20.55	15.7134 ± 91	15.71	39.975 ± 39	39.94	-0.90	-53.9	447	416
Chatham Islands																
P80180[2]	0.0911	0.2972	0.2197	27.9	0.202	92.5	20.801 ± 11	20.44	15.7590 ± 34	15.74	40.235 ± 15	39.85	1.31	-54.1	279	256
P80290[1]	0.0403	0.1176	0.0173	163.0	1.18	484.5	22.433 ± 14	20.29	15.8369 ± 38	15.74	41.817 ± 18	39.80	-8.59	-93.2	112	115
P80291[2]	0.1074	0.4444	0.4175	16.7	0.121	70.5	19.514 ± 13	19.29	15.6708 ± 75	15.66	39.130 ± 25	38.84	6.44	-8.93	--	21.2
P80354a[1]	0.0049	0.0092	0.0167	19.2	0.139	36.7	19.914 ± 6	19.72	15.6863 ± 27	15.68	39.2346 ± 92	39.12	3.66	-46.8	115	97.9
P80354b[1]	0.0037	0.0094	0.0103	23.6	0.171	60.9	20.041 ± 11	19.81	15.7217 ± 59	15.71	39.435 ± 19	39.25	5.83	-42.1	128	125
P80354c[1]	0.0050	0.0108	0.0222	14.8	0.108	32.4	19.919 ± 7	19.77	15.7126 ± 45	15.71	39.182 ± 13	39.08	6.24	-52.7	151	78.1

Table 3: Errorchron age estimates of Zealandia lithospheric metasomatism

Locality	Type [A]	^{238}U-^{206}Pb system Age (Ma)	*MSWD*	^{235}U-^{207}Pb system Age (Ma)	*MSWD*	^{232}Th-^{208}Pb system Age (Ma)	*MSWD*	n [B]	Weighted Average	Basis for exclusion [C]
Chatham Islands	All-inclusive:	110 ± 54	*1810*	121 ± 81	*22*	115 ± 52	*172*	6 (6)	114 ± 33	Small scale heterogeneity
	Preferred:	110 ± 9.3	*20*	119 ± 77	*7.5*	115.9 ± 3.1	*2.8*	4	**115.3 ± 2.9**	
Fortification Peak	All-inclusive:	54 ± 36	*415*	51 ± 51	*28*	63 ± 24	*184*	7 (6)	59 ± 18	Preserved ancient heterogeneity
	Preferred:	72 ± 10	*350*	74 ± 23	*15*	67.1 ± 5.7	*54*	6	**68.6 ± 4.7**	
Pilot Point	All-inclusive:	31 ± 33	*9820*	40 ± 83	*360*	22 ± 19	*1590*	8 (5)	25 ± 16	Lack of equilibrium: whole rock vs. cpx
	Preferred:	41.5 ± 9.1	*220*	68 ± 32	*30*	28.3 ± 3.5	*33*	6	**30 ± 18**	
Trig L	All-inclusive:	30 ± 110	*86*	36 ± 17	*0.91*	25 ± 21	*3.9*	6 (4)	32 ± 13	Large offset in $^{206}Pb/^{204}Pb$
	Preferred:	26 ± 15	*71*	36 ± 17	*1.16*	24 ± 31	*5.1*	5	**30 ± 10**	

Figure 1

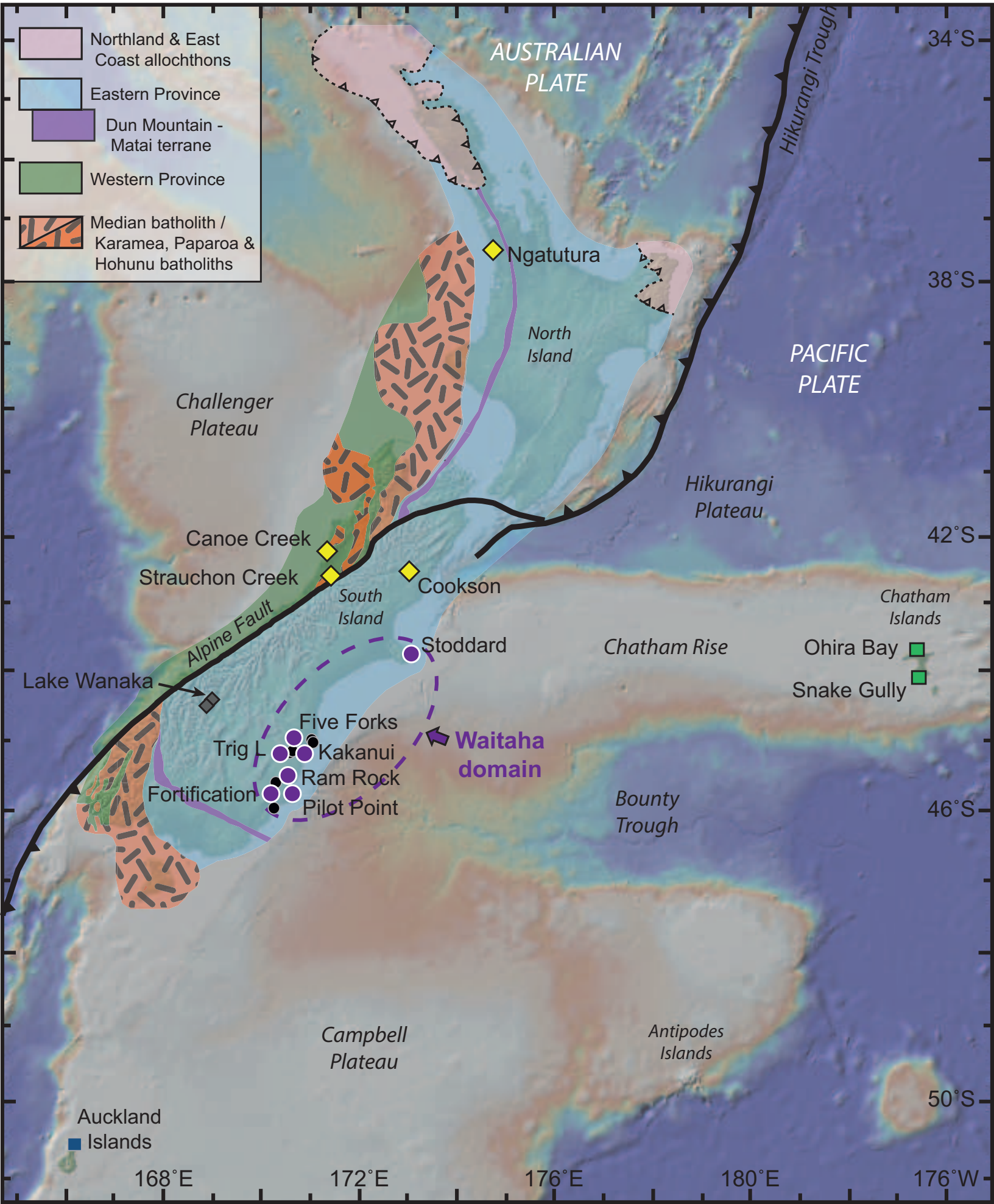

Figure 2

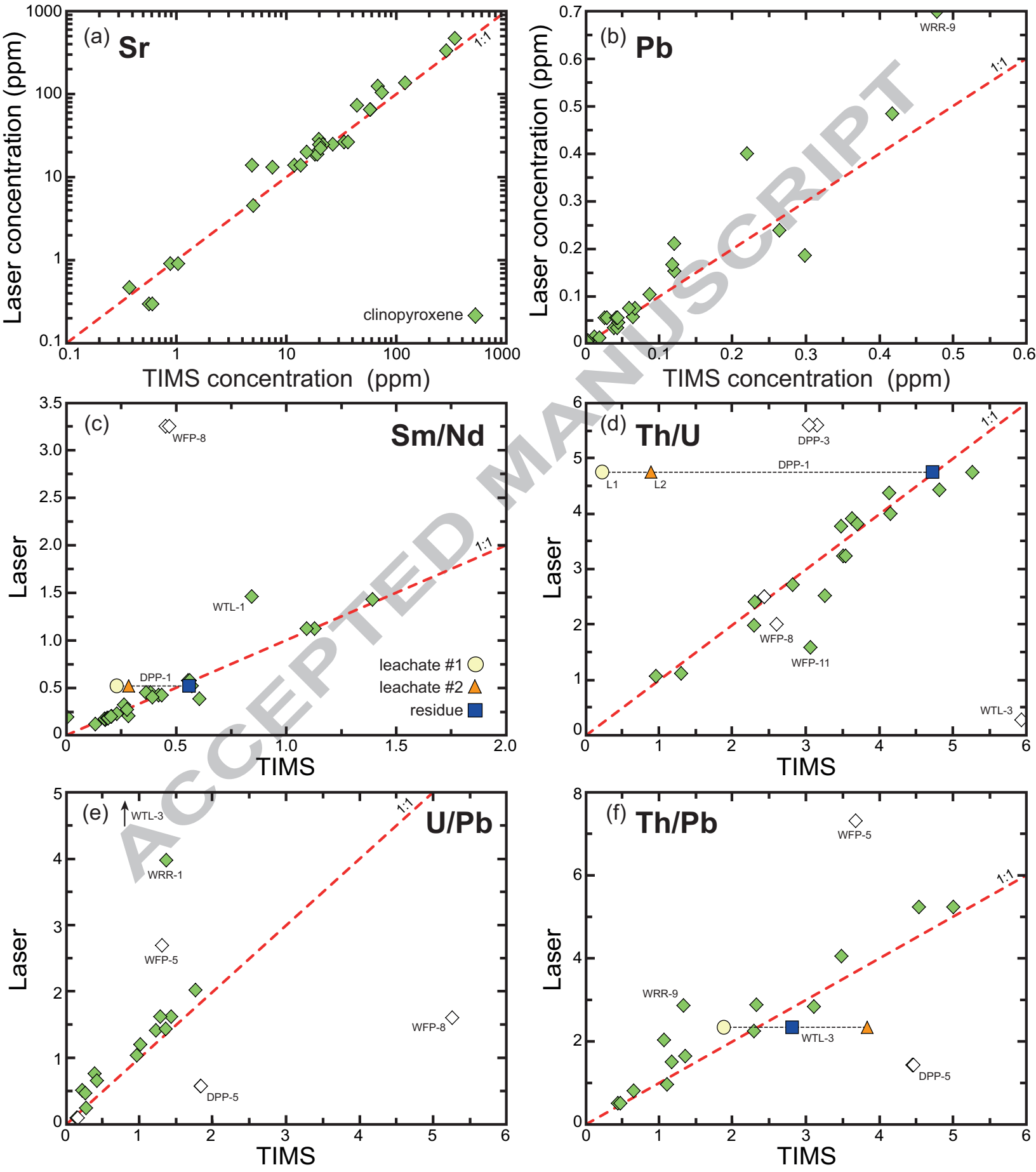

Figure 3

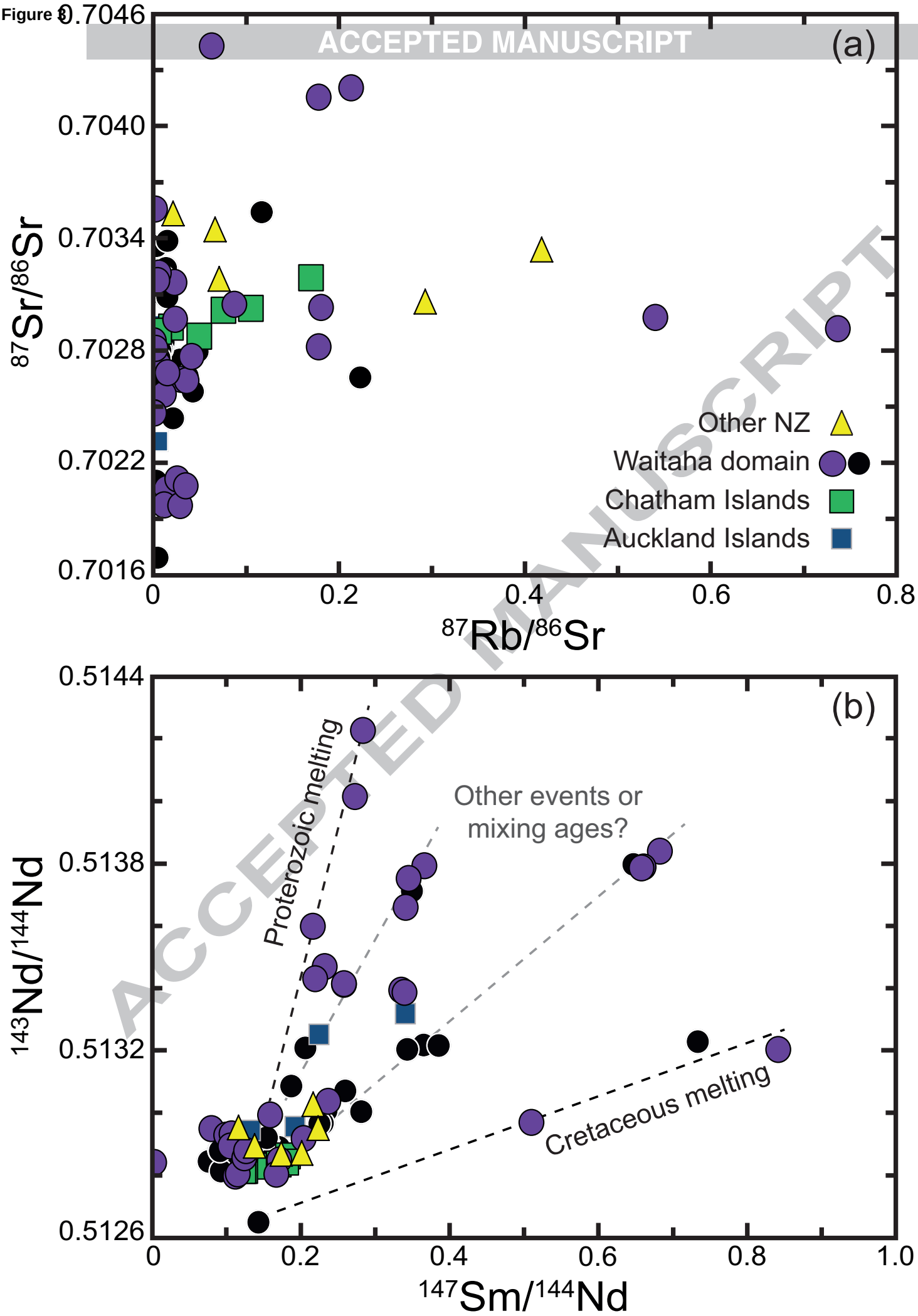

Figure 4

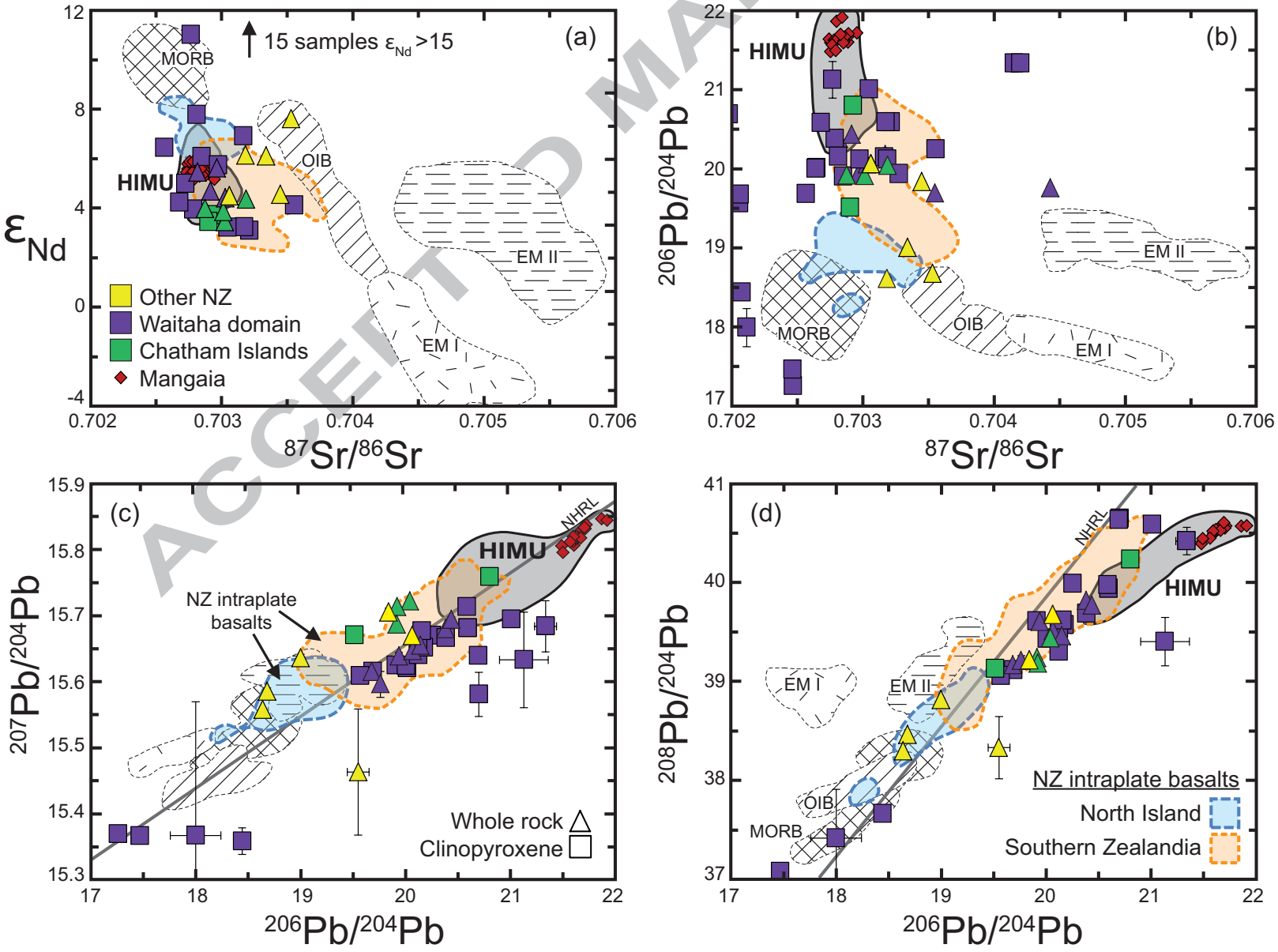

Figure 5

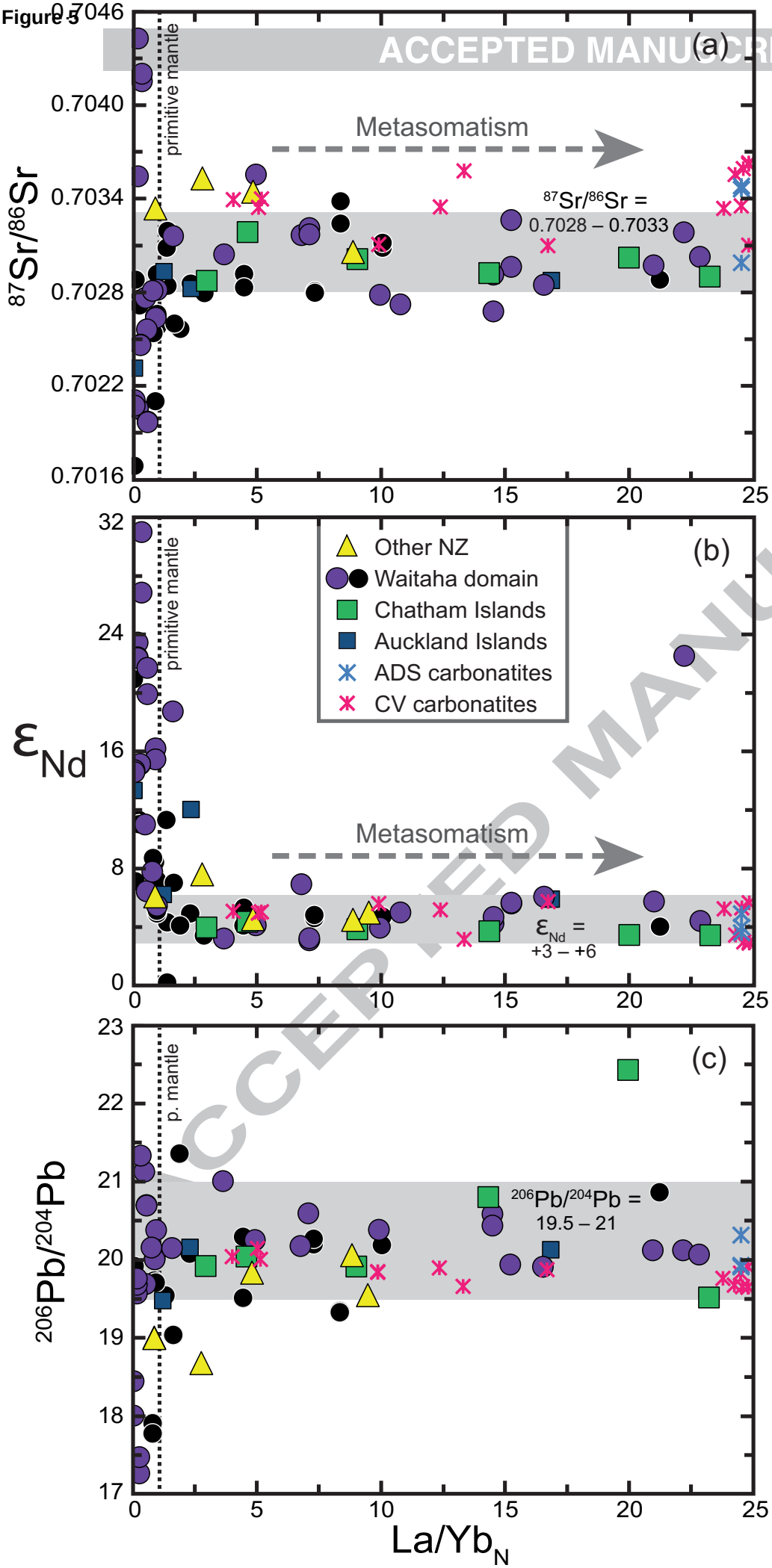

Figure 6

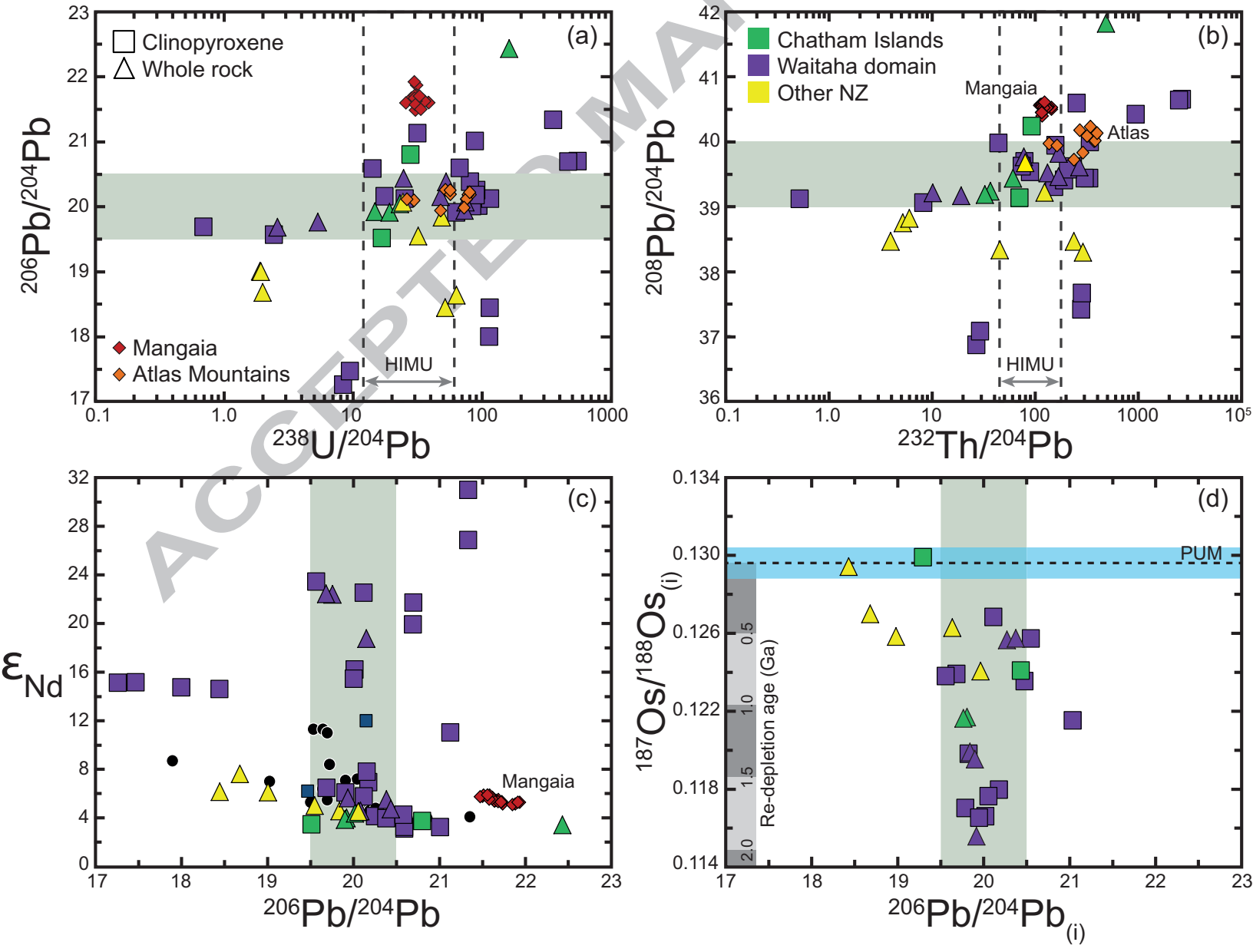

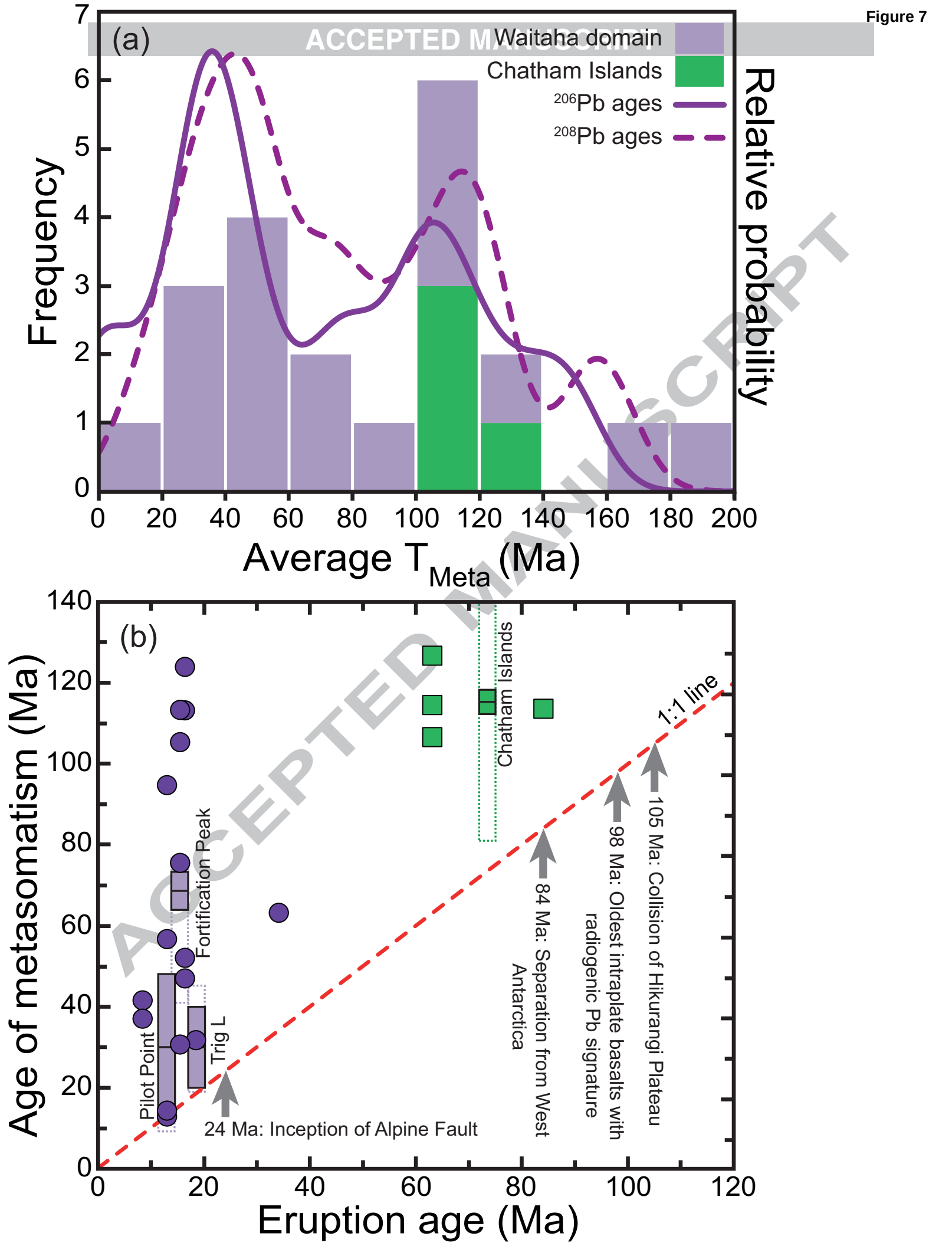

Figure 8

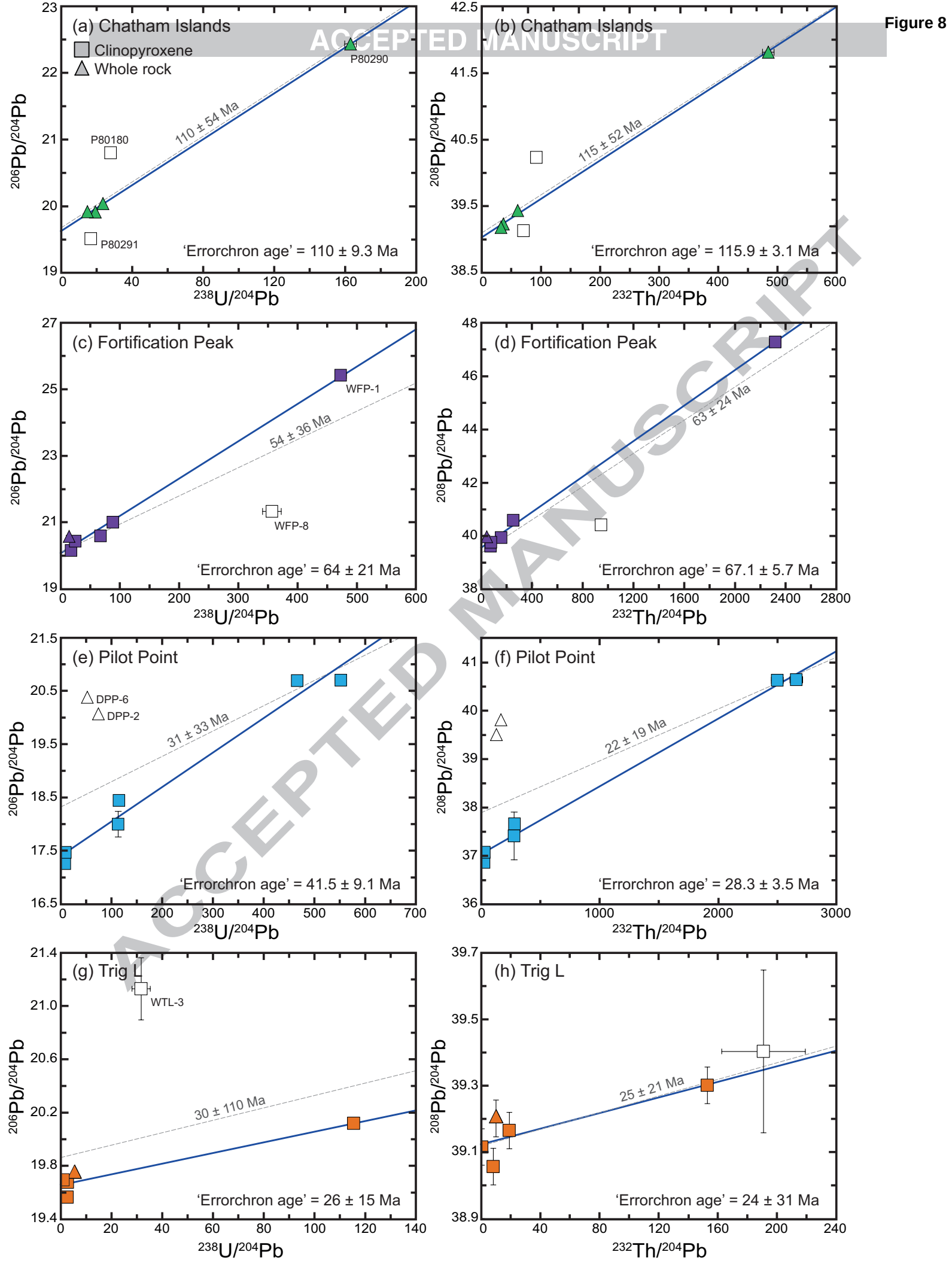

Figure 9

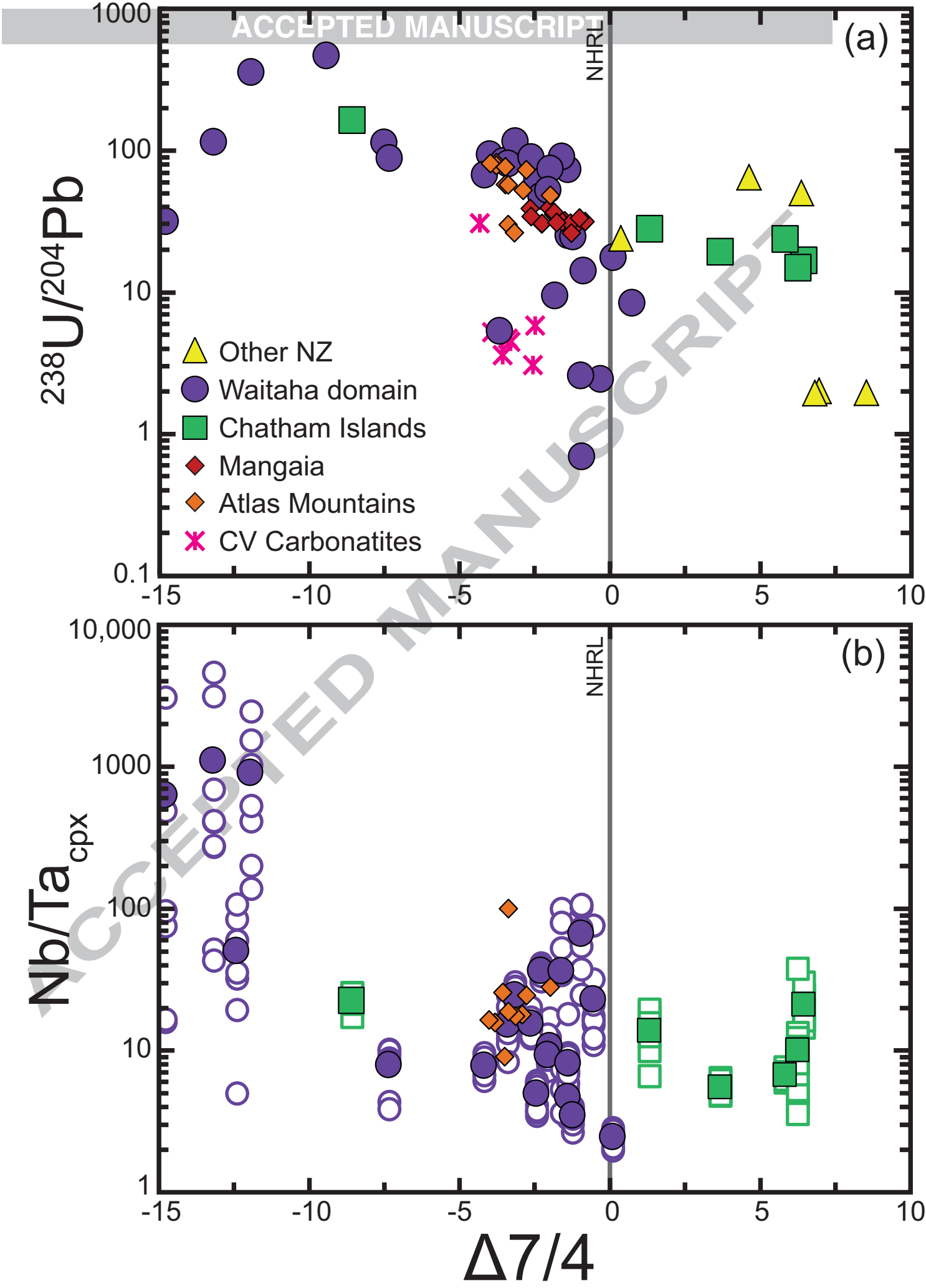
ACCEPTED MANUSCRIPT
(a)
NHRL
$^{238}U/^{204}Pb$
1000
100
10
1
0.1
-15
-10
-5
0
5
10
Other NZ
Waitaha domain
Chatham Islands
Mangaia
Atlas Mountains
CV Carbonatites
(b)
NHRL
Nb/Ta_{cpx}
10,000
1000
100
10
1
Δ7/4
ACCEPTED MANUSCRIPT

Figure 10